Faculdade de Tecnologia
Universidade de Brasília

Desenvolvimento de Dispositivo para Dobra de Chapas Metálicas: Simulação em Elementos Finitos, Concepção e Sistema de Controle

Eduardo Perez Liberato

TRABALHO DE GRADUAÇÃO

ENGENHARIA MECATRÔNICA - CONTROLE E AUTOMAÇÃO

Brasília

2023

Faculdade de Tecnologia
Universidade de Brasília

Metal Sheet Bending Device's Development: Finite Element Analysis, Conception and Control System

Eduardo Perez Liberato

Trabalho de Graduação submetido como requisito parcial para obtenção do grau de Bacharel em Engenharia Mecatrônica - Controle e Automação.

Orientador: Prof. Dr. Lucival Malcher

Brasília
2023

Liberato, Eduardo Perez.
L695d Desenvolvimento de Dispositivo para Dobra de Chapas Metálicas: Simulação em Elementos Finitos, Concepção e Sistema de Controle / Eduardo Perez Liberato; orientador Lucival Malcher. -- Brasília, 2023.
73 p.

Trabalho de Graduação em Engenharia Mecatrônica - Controle e Automação -- , 2023.

1. Dispositivo de Dobra. 2. Método dos Elementos Finitos. 3. Fabricação de Projeto. 4. Sistema de Controle. I. Malcher, Lucival, orient. II. Título

Faculdade de Tecnologia
Universidade de Brasília

Desenvolvimento de Dispositivo para Dobra de Chapas Metálicas: Simulação em Elementos Finitos, Concepção e Sistema de Controle

Eduardo Perez Liberato

Trabalho de Graduação submetido como requisito parcial para obtenção do grau de Bacharel em Engenharia Mecatrônica - Controle e Automação.

Trabalho Aprovado. Brasília, 10 de Fevereiro de 2023:

Prof. Dr. Lucival Malcher, UnB/FT/ENM
Orientador

Profa. Dra. Déborah de Oliveira, UnB/FT/ENM
Examinador interno

Prof. Dr. Leonel Delgado Morales, Universidad Austral de Chile
Examinador externo

Brasília
2023

Acknowledgements

Firstly, I would like to thank my mother and my father for all the emotional and financial support they provided me during my graduation in Engineering. Additionally, I thank them for giving me an environment where I could improve my studies and have contact with various experiences throughout my life.

Secondly, I would like to thank Professor Dr. Lucival Malcher for his guidance and all the support he provided since when I asked for his help to have an idea of a graduation work. I also thank him for his time and his teachings, including the opportunity to participate in his classes in Solid Mechanics and Finite Element Method.

A very special thank to my girlfriend, future lawyer Maria Eduarda Martins Santos e Silva, who had patience with me during this work. She also has been my lovely companion for many hours each week during the last three years, being sweet and attentive.

I would like to thank Professor Dr. Déborah de Oliveira for helping me with ideas on manufacturing parts. In addition, I thank her for instructing me while I was her assistant during her classes of Manufacturing Technology 1, specially on the use of numerical control machines and methods for manufacturing parts.

I would also like to thank current students and future engineers João Pedro Cardoso Finamore Ivo, Rodrigo Brant Lobato, and Isabela Maria Pereira Cruzeiro for facilitating my understanding in the areas of Electrical, Mechanical, and Control Engineering, respectively. In addition, I would like to thank the opportunity to count on many people of different backgrounds throughout my academic career at the University of Brasilia (UnB). Some of these names supported me throughout this time and should be mentioned, such as: Rodrigo Villar Raposo, Ana Júlia Brant Lobato, Abraão Alves Braga, Gustavo Nakandakari de Oliveira, Gabriel Tardelli Ciuffo Moreira (future engineers), Deocleciano Ferreira Rios Neto, Felipe de Almeida Menezes (current president of the junior company Tecmec, at UnB), Bianca Maria Guedes Trotta (future designer), Hugo da Costa Melo Gomes Ferreira (mechanical engineer graduated from UnB), and Ricardo Alexandre Garcia Alves (future lawyer who helped me to revise the wording of this work).

At last, but not at least, I would like to thank Dimitri Gabriel Chaves Gomes, electromechanical technician, for giving me tips and teachings on how to properly use the AutoCAD tool, as well as Adriano Ricardo Lopes and Rafael Silva Barros for helping me in manufacturing processes, both technicians currently working in SG-9 Laboratory in the UnB.

"What I'd like to talk about is a part of physics that is known, rather than a part that is unknown. People are always asking for the latest developments in the unification of this theory with that theory, and they don't give us a chance to tell them anything about one of the theories that we know pretty well. They always want to know things that we don't know. So, rather than confound you with a lot of half-cooked, partially analysed theories, I would like to tell you about a subject that has been very thoroughly analysed."
(Richard P. Feynman)

Abstract

Metal bending is a manufacturing process widely used in aerospace, automotive, metallurgical and construction industries. The objective of this project is the development a device capable of provide this bending. Initially it involved a study of the device's design, including technical drawings. Finite element simulations were then performed to verify the design sizing. The development also included the beginning of the device manufacturing to provide a physical system to perform the bending of the metal sheets. Finally, a control system is proposed to be implemented for this device to measure the force applied to the sheets. AutoCAD software was used during the device designing, Abaqus software was applied during finite element simulation, and Arduino integrated development environment platform was employed to build the algorithm to collect sensor data to monitor the force during the bending event. This project can be classified as a preview of a digital representation of a metal sheet bending device. It presents simulations using finite element analysis and a similarity verification of the physical system to its digital version.

Keywords: Bending device. Finite Element Analysis. Project's Manufacturing. Control System.

Resumo

O dobramento de metais é um processo de fabricação amplamente utilizado nas indústrias aeroespacial, automotiva, metalúrgica e de construção. O objetivo deste projeto é o desenvolvimento de um dispositivo capaz de fornecer este dobramento. Inicialmente, houve um estudo do design do dispositivo, incluindo desenhos técnicos. Simulações em elementos finitos foram realizadas para verificar o dimensionamento do projeto. O desenvolvimento também incluiu o início da fabricação de dispositivos para fornecer um sistema físico para executar a dobra das chapas metálicas. Finalmente, é proposto que um sistema de controle seja implementado para este dispositivo medir a força aplicada às chapas. O *software* AutoCAD foi usado durante o design de dispositivos, o *software* Abaqus foi aplicado durante a simulação em elementos finitos e a plataforma de ambiente de desenvolvimento integrada do Arduino foi utilizada para criar o algoritmo de coletar dados do sensor a monitorar a força durante o evento de dobra. Este projeto pode ser classificado como uma prévia de representação digital de dispositivo de dobra de chapas metálicas. Apresenta simulações usando análise em elementos finitos e uma verificação de similaridade do sistema físico para sua versão digital.

Palavras-chave: Dispositivo de Dobra. Método dos Elementos Finitos. Fabricação de Projeto. Sistema de Controle.

List of Figures

List of Tables

Contents

1 Introduction

1.1 Contextualization

Metal bending is a manufacturing process widely used in aerospace, automotive, metallurgical and construction industries, as shown in (BARRANS; MULLER, 2009), (BISAGNI et al., 2022) and (BOUKAR et al., 2022). Bending manufacturing products can be found, for example, in auto parts, water pipes, wire support profiles and aircraft wings, as presented in (BOUVET; VIEILLE; PUJOLS-GONZALEZ, 2022).

The bending process is also be applied in the biomedical field in order to help the development of new treatments for diseases related to skeletal fragility, such as osteoporosis, as shown in (RIDHA; THURNER, 2013). These treatments can be improved with new material design that has a higher level of resistance to fractures and that can be easier implanted in the patient. Additionally, sheet metal bending metal bending devices can improve mechanisms for treating human bone fractures, as introduced in (SÖNTGEN et al., 2022). Another bending process medical application can be found in materials testing for the development of catheters, as presented in (BADROU et al., 2022).

To perform a bend in a metal sheet it is necessary to have proper devices made to do this type of manufacturing. The development of these devices requires analyses involving their mechanical components subject to stresses and to displacement. Finite element method can be used for these analyses (HINCHY et al., 2020).

There is an effort to simulate part of the process of bending through finite element analysis used for digital prototyping of the functioning of a device. In this sense, the ideal model is a perfect digital representation of a physical system, known as “digital twin” (HINCHY et al., 2020). It can be used to predict a material elastic modulus, since it is possible to compare physical testing with a finite element representation, as presented in (ÖZEN et al., 2021). Digital twins are also associated with simulations of large structures that might experience failures, such as wind turbine blades, as shown in (EDER; CHEN, 2020), and reinforced concrete beams, as presented in (BLOMFORS; LUNDGREN; ZANDI, 2020).

1.2 Objectives

The objective of this project is the development of a metal sheet bending device, comprising its design, simulations, manufacturing, and control system. Initially, it is presented the design of the metal sheet bending device. Once defined the dimensions of the device

and its components, the next intermediate objective consists in determining the maximum force that the device can withstand using an analysis of the bending process. The subsequent intermediate objective is to start the manufacturing of the device. The final intermediate objective is to implement an electronic system that will monitor the bending force from data collected through a sensor and processed by an Arduino board.

The project aims to contribute to the validation of material failure tests and to the development of device projects. It also intents to help studies involving plasticity, mechanics of materials, and mechanical equipment control. Considering that the device is lightweight, easy to transport, and designed to produce bending on small-scale metal sheets (100x100x4 mm), this project can be a facilitator for academic disciplines to train future engineers. With several and different simulations, this work may contribute to the study and the validation of mechanical components' sizing using finite element analysis.

1.3 Organization

Initially, a literature review is presented in chapter 2, which contains information related to this work, such as the process of bending metal sheets and how to predict, from an equation, the force required to bend a metal sheet.

The next chapter, chapter 3, is related to the methodology of the work, exposing how each step is carried out and providing information on the adoption of methods and materials.

The subsequent chapter, chapter 4, reveals which parameters are considered to the simulations, the results of the bending process, and the aspects of the bending phenomenon that are relevant to the device's assembly.

The manufacturing of the device is dealt in chapter 5, focused on the assembly of the physical equipment, presenting topics on its components' machining and welding.

Once considering the device is physically ready to bend a metal sheet, chapter 6 presents an Arduino integrated development environment (IDE) platform with its board connected to a sensor that is also attached to the metal bending device. This sensor will monitor the bending force.

Finally, chapter 7 presents the conclusion, exhibiting the main results of the mentioned simulations, as well as considerations on the device assembly and a proposition regarding its control system. This chapter also presents possible future actions related to this project and recommendations to upcoming works on the issue.

2 Literature Review

This project uses theoretical concepts used for various purposes in industries, such as sizing of structures based on material failure criteria and control systems. For instance, these concepts are used to analyse the appropriate length of a wind turbine blades, as presented in (EDER; CHEN, 2020). This chapter covers theoretical concepts used in this project as it follows.

2.1 Metal Sheet Bending Devices

The literature on metal sheets bending devices presents and analyses these machines considering, among other aspects, the diversity of their size. The machine used in this project was originally inspired in a small device as presented in (HINCHY et al., 2020) (illustrated in Figure 1). Metal bending devices with computerized numerical control (CNC), which performs tests based on an algorithm on a computer, usually are larger machines, as presented by (MORI; AKITA; ABE, 2007) (depicted in Figure 2).

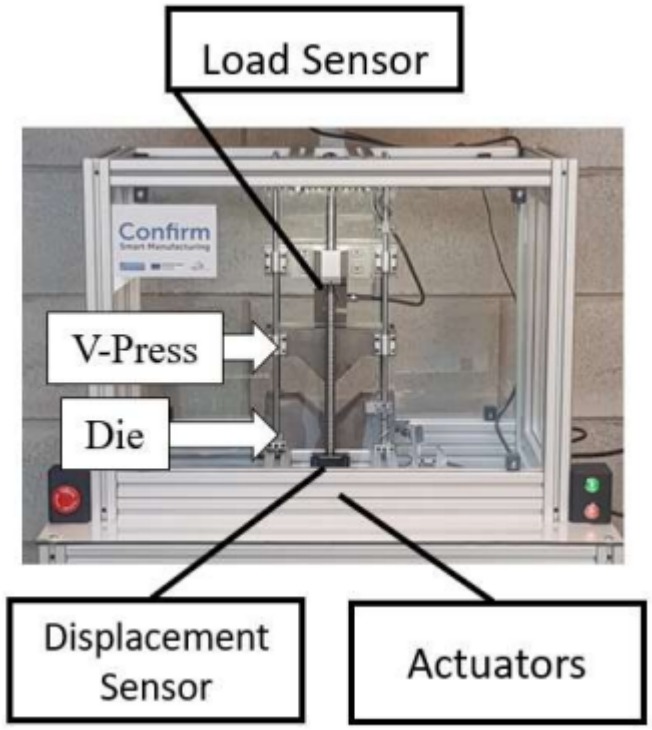

Figure 1 – Metal Sheet Bending Machine Model proposed by (HINCHY et al., 2020).

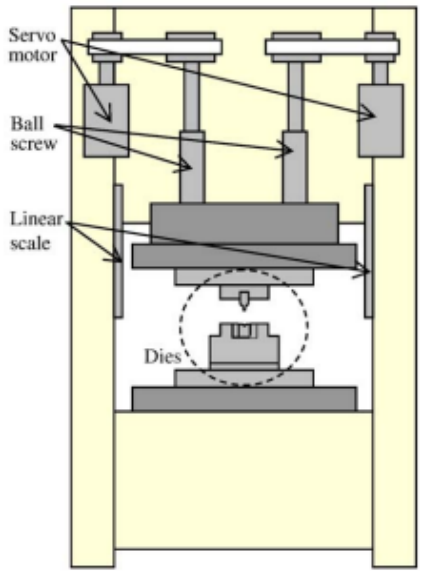

Figure 2 – Metal Sheet Bending Machine Model proposed by (MORI; AKITA; ABE, 2007).

2.2 Analytical Equation of the Force Required to Bend a Metal Sheet

This section presents how the force required to bend a metal sheet can be determined. The equation below, shown in (KALPAKJIAN; SCHMID, 2006), describes how the force required for the bending process of a sheet can be obtained:

$$F_{max} = k \cdot \frac{UTS \cdot L \cdot t^2}{W} \tag{2.1}$$

In which F_{max} is the maximum force to be measured, k is a constant that can vary between 2,4 and 2,6, UTS is the ultimate tensile strength of the material, L is the sheet's length, t is the sheet's thickness, and W is the opening length in the "V"-die where the metal sheet will be bent.

2.3 Stress and Strain

The definition of stress is presented in (HOSFORD, 2005), which is the intensity of force at a point. Since the stress state (σ) is the same throughout a body, assuming that force is represented by the letter F and area by the letter A, it can be deduced that:

$$\sigma = \frac{\partial F}{\partial A} = \frac{F}{A} \tag{2.2}$$

On one hand, when a material is deformed by small stresses and return to its original state, this action can be classified as an elastic deformation. On the other hand, if the material

is permanently deformed, and does not return to its original shape, plastic deformation occurs.

Additionally, it is worth mentioning the difference between normal stress, perpendicular to the object's plane, and shear stress, parallel to the plane where the object is located.

2.4 Material Failure Criterion

The Von Mises criterion suggests that the material must have a distortion energy value per unit volume of the material less than the same energy that causes the flow of the specimen in the material ($u_d < u_{d_e}$). Thus, the equation used to find the energy u_d can be written as:

$$\frac{1}{6G} \cdot (\sigma_1 - \sigma_2)^2 + (\sigma_2 - \sigma_3)^2 + (\sigma_3 - \sigma_1)^2 = u_d < u_{d_e} = \frac{\sigma_e^2}{6G} \tag{2.3}$$

The above equation puts the values of σ_1, σ_2 and σ_3 as the stresses on the x, y and z axes of the Cartesian coordinates, considering (HOSFORD, 2005). The constant G in the above equation is the modulus of the material's elasticity. Hence, one can define the Von Mises failure criterion as follows:

$$(\sigma_1 - \sigma_2)^2 + (\sigma_2 - \sigma_3)^2 + (\sigma_3 - \sigma_1)^2 < 2 \cdot \sigma_e^2 \tag{2.4}$$

Where the variable σ_e means the yield stress of the material.

2.5 Finite Element Method

As previously mentioned, the finite element method is commonly used in various Engineering fields, since it is possible to analyse quantitative variables throughout an object. For example: stresses in a bending sheet, shown in (HINCHY et al., 2020), or in a reinforced concrete beam, presented in (BLOMFORS; LUNDGREN; ZANDI, 2020). This work uses the finite element method employing an Abaqus software computational analysis.

Hence, all information used in this work is implemented following the suggestions of the Abaqus manual - (ABAQUS, 2011). This software can provide simulations of different materials. A simulation similar to this work is presented in (VORKOV et al., 2014), in which a steel sheet was submitted to a bending process and the simulations of its bending were carried out in a three-dimensional way.

In the current work the sheet bending was made of aluminium and two-dimensional simulations were performed, although it was done an additional simulation in three dimensions of the external structure of the bending device, that is called chassis.

2.6 Manufacturing Processes Performed in this Work

Conventional machining processes were used in this work. Machining is a subtractive manufacturing process, since it is a material-removal process to obtain a desired part, and can be classified into:

- Conventional processes, such as turning, drilling, milling, and sawing (using specific tools), as well as grinding (abrasive process).
- Unconventional processes, such as abrasive jet and laser cutting.

The manufacturing phase of the bending device in this work used milling machines, a lathe, a drill press, a grinder, a disk saw, and a rotary brush from the SG-9 Laboratory in the University of Brasilia (UnB). The information presented in this section is based on the graduation works of (BARRETO, 2022) and (ÁVILA, 2022).

Furthermore, welding (a material deposition manufacturing process) was used in this work, as presented in (KALPAKJIAN; SCHMID, 2006). This graduation project used welding on metal inert gas (MIG) and on coated electrode.

2.7 Closed-Loop Control System

The closed-loop control system, presented in (OGATA, 2011), is a system in which the input signal - $R(s)$ - is transformed by a controller - $C(s)$ - and a plant - $P(s)$. The output - $Y(s)$ - serves as a "feedback" to the summing block, controlling the device. Thus, as shown in the Figure 3, one can write that:

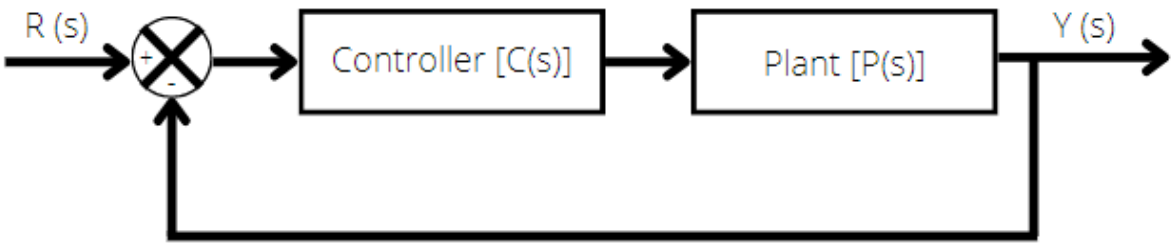

Figure 3 – Simple controller model with negative unitary feedback.

This control system, as a whole, has a transfer function that can be written as $G(s)$, being the ratio between the output and input of the block diagram presented in Figure 3, which can be given by the equation:

$$G(s) = \frac{Y(s)}{R(s)} = \frac{C(s) \cdot P(s)}{1 + C(s) \cdot P(s)} \tag{2.5}$$

The approach of a closed-loop control system can be solved by a state-space analysis, in which a physical system is represented in matrix format. However, a simple block diagram will be used as the chosen system for monitoring the physical system force is a single-input single-output (SISO) system.

2.8 Wheatstone Bridge

The Wheatstone bridge is a type of voltage divider that becomes a sensor by having a variable resistance (as shown in Figure 4) on one side and a constant resistance on the other side . When the sensor is put into operation, it generates a voltage between the side of the bridge that has a variable resistance and the side of the bridge that has a constant resistance, as (BENTLEY, 2005) explains.

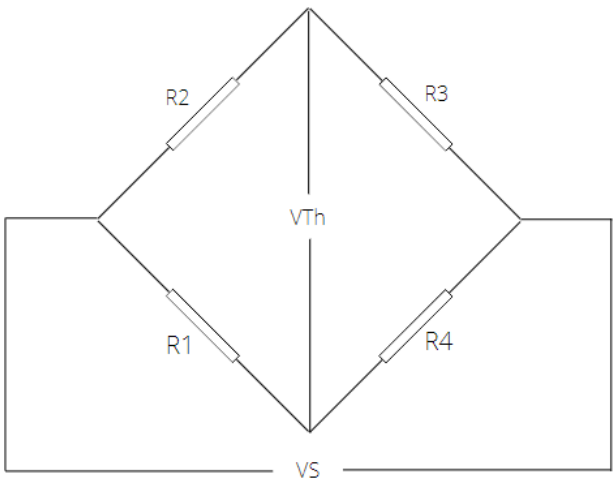

Figure 4 – Schematic drawing of the Wheatstone bridge with the resistors.

Thus, it can be stated that the value of the voltage to be measured (V_{Th}), due to the voltage divider is:

$$V_{Th} = V_S \cdot \left(\frac{R_1}{R_1 + R_4} - \frac{R_2}{R_2 + R_3}\right) \tag{2.6}$$

Where V_S is the circuit power supply voltage, R_1 is the variable resistance 1, R_2 is the constant resistance 2, R_3 is the constant resistance 3, and R_4 is the constant resistance 4. Normally even on the variable side, only one resistor has a variable resistance. Considering K a constant, it can be written that:

$$K = \frac{R_2}{R_2 + R_3} \tag{2.7}$$

$$V_{Th} = V_S \cdot \left(\frac{R_1}{R_1 + R_4} - K\right) \tag{2.8}$$

3 Methodology

This chapter presents the methods used in this work to achieve the main and the intermediates objectives indicated in chapter 1. For this purpose, some of the published works mentioned in the literature review in chapter 2 were used.

Firstly, the conception of the project, exhibiting dimensions proposed by the project and technical drawings, is presented in chapter 4. During the next step, the design phase, Abaqus software was used to simulate the bending process and to calculate the maximum force to accomplish the bending process of metal sheets with different thicknesses. The force applied by the actuator on the internal surface of the chassis was calculated to verify whether this chassis, the mould, and the punch could withstand the calculated stresses. The maximum value of this force was predicted by the simulations using the finite element analysis.

After completing the project simulations, chapter 5 presents the manufacturing work in order to build the bending device, including grinding and iron oxide removal process of mechanical components, use of manual milling and drilling machines, employment of CNC milling machines, welding of parts, and heat treatment seeking to improve component rigidity.

The next chapter, chapter 6, demonstrates how the force monitoring system is going to be implemented in the bending device. It is presented how electronic components are connected to each other and how they are also connected to the mechanical structure of the bending device. These components consist of:

- A sensor, an electronic board capable of receiving and inform voltage variation, acting as a Wheatstone bridge.
- An Arduino module.
- A series of wires to make the interconnection of each electronic part of the planned system.

At the end of chapter 6, it will be shown how the sensor calibration will be performed using an algorithm that will be built in the Arduino IDE. This code, once calibrated, should continuously update, and inform the force being applied during the simulation of a system while performing a bending event.

4 Conception and Sizing of the Project

Initially, the project was based on the idealization of activating a hydraulic actuator with a single-acting cylinder and spring return, as shown in Figure 5. The actuator used was a RC-51 model, available in SG-9 Laboratory in UnB. It has a maximum forward of 25 mm, according to (ENERPAC, 2022). Considering this type of actuator, some sketches were made to design a chassis that would support the forces present in the bending event. If the actuator is activated it advances downwards, applying a force in the same direction as the gravity's acceleration. Hence, the actuator would be attached to the bending device structure's upper part.

Figure 5 – Photo showing the Enerpac's RC-51 actuator used in this project.

A punch being pushed against a metal sheet causes a plastic deformation in the sheet, according to the "V" recess made in the mould, and leading to the completion of the sheet metal bending process. Therefore, initially it was pondered that a punch would be connected at the bottom of the actuator (the part which will advance against the metal sheet).

Given the project concept, it can be shown that the project design is a structure formed by 4 cylindrical bars mounted between two plates, and a trapezoidal component mounted above the upper plate to improve the chassis rigidity. As mentioned before, the actuator would be attached to superior part of the device. The technical drawings of the parts of the project can be found in Appendix A.

Once the technical drawings are completed, details of the device design will be presented in the following section, including the development of the components using Abaqus software with the intention of simulating these drawings.

4.1 Project Design

The work was focused on the development of a small, lightweight, and easy to manufacture device that can be used for academic work. According to the technical drawings available in Appendix A, the bottom plate is designed with dimensions of 300 mm in length, 20 mm in height, and 100 mm in depth. The top plate is a reproduction of the bottom one in order to facilitate its manufacture, as shown in Figure 6. In addition, the cylindrical bars are solid and identical. They have a height of 212 mm and their circular section have an individual radius of 7,5 mm, as can be seen in Figure 7.

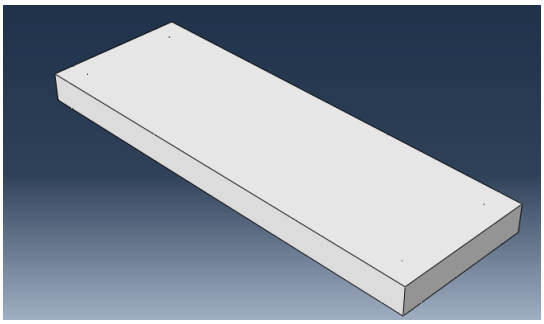

Figure 6 – Models of the plates and auxiliary plate used in the project's simulation.

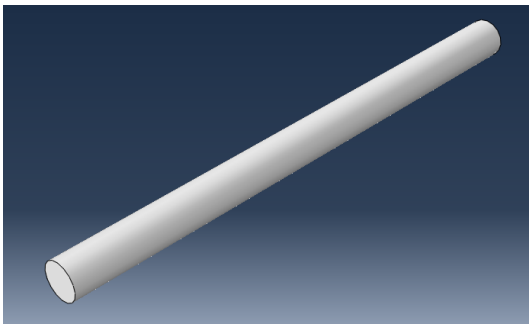

Figure 7 – Cylindrical bars model used in the project's simulation

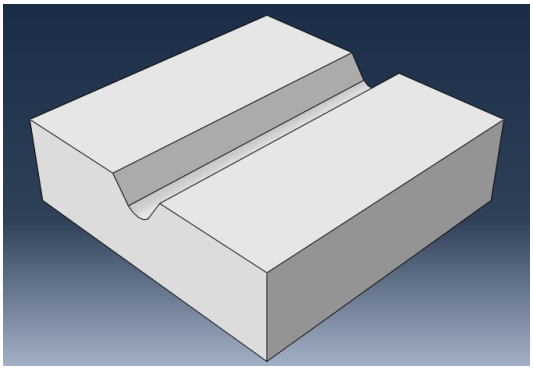

Figure 8 – Project's mould.

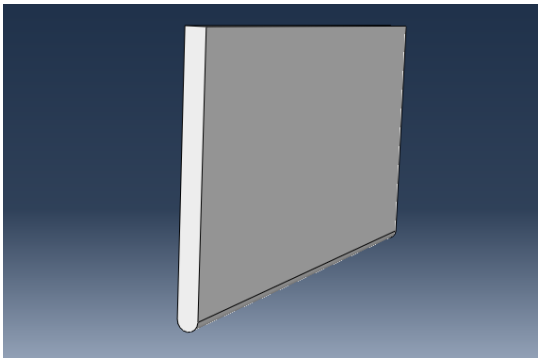

Figure 9 – Project's punch

The mould to shape the metal sheet bend is designed to have height, base, and depth dimensions of 30 mm, 100 mm, and 100 mm, respectively, as displayed in Figure 8. Moreover, the mould has a "V"-die in its middle (where the punch pushes the metal sheet against it, deforming it).

During technical drawings and simulations, the bending angle in the "V"-die in the mould varies according to the thickness of the sheet metal to be bent. The distances from the minimum point of the "V" recess were defined in such a way that the punch, pushed by the actuator shown in Figure 5, would always be at a final displacement of 10 mm from its initial point, considering the load limitation of the RC-51 actuator.

The punch (shown in Figure 9) was initially designed to be a piece with a height of 50 mm, a width of 4 mm, and a depth equal to that of the mould, 100 mm. In a frontal view

its tip is rounded with a circle of radius 2 mm. The punch has a reference point placed on its top to obtain data on the force variation suffered in this point during the bending process.

4.2 Project's Sizing

After the presentation of the mechanical components, finite element analysis was performed to verify whether these components could withstand the maximum load applied to the chassis, the punch, and the die by the RC-51 actuator. The maximum load that the actuator can provide is the highest load to be applied to metal sheet which will be bent with a certain thickness.

It is worth noting that the failure criterion chosen to verify the highest stress measured in the simulations is the von Mises failure criterion, commonly mentioned in the literature and in projects found in industries.

4.2.1 Determination of Bending Machine's Maximum Force to be Supported

The simulations used sheets made of aluminium. It was also assumed that the chosen material had the following parameters, found in (MALCHER et al., 2020), presented in Table 1 and Table 5, the latter is on the Appendix B.

The sheets used in the Abaqus simulations were AA6101-T4 aluminium sheets with varying thicknesses - 1 mm, 2 mm, 3 mm and 4 mm. These sheets had the following properties, shown in Table 1:

Table 1 – Metal conditions used to perform the simulations in order to verify the bending process

Metal's name	Young's Modulus (E [GPa])	Poisson's Ratio (υ)	Density ($[kg \cdot m^{-3}]$)
Aluminum AA6101-T4	70	0.3	2700

Source: (MALCHER et al., 2020)

In addition, it was ensured that the material would go into plastic deformation and did not break by using a strain-hardening curve. The plastic deformation of an aluminium sheet was obtained from the data in Table 5, which was found in (MALCHER et al., 2020).

According to the variation in the metal sheets' thickness, different forces were calculated in each Abaqus simulation. Thus, Table 2 relates this thickness to the resulting force required to bend the metal sheet without affecting its thickness, this resulting force was collected from the reference point on the punch.

The results for the simulations, using a *quad* mesh and with a variation of at least 1600 and at most 6400 elements for the representations of the metal plates, were exhibited in Figure 10, Figure 11, Figure 12 and Figure 13.

Table 2 – Forces applied to bend metal sheets during the simulations.

Metal Sheet Thickness [mm]	Maximum Numerical Force [N]	Load [ton]
1	11266	1,15
2	20648	2,12
3	35484	3,62
4	48294	4,93

Source: (ABAQUS, 2011)

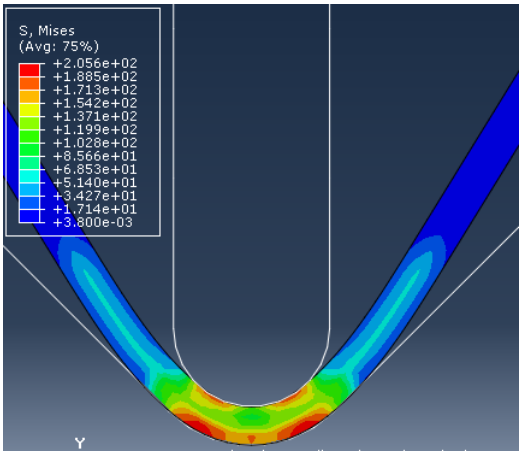

Figure 10 – Stress distribution in a 1 mm metal sheet bended.

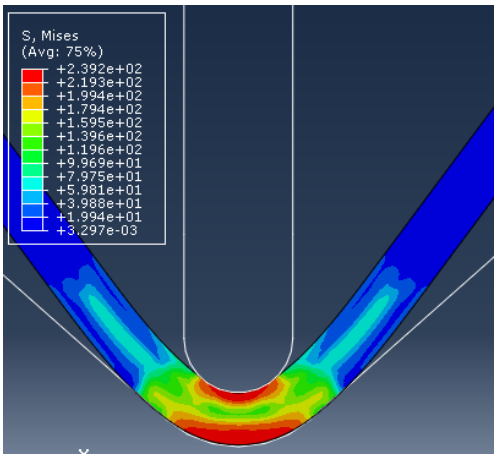

Figure 11 – Stress distribution in a 2 mm metal sheet bended.

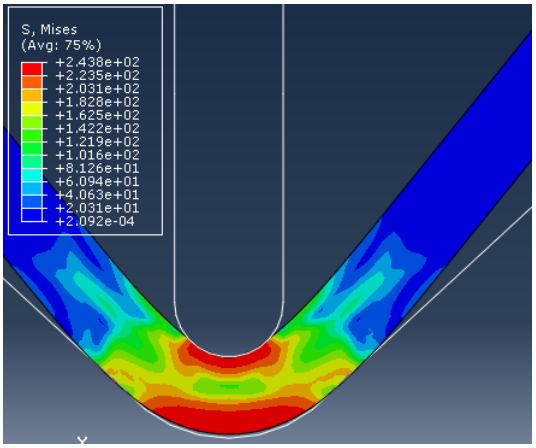

Figure 12 – Stress distribution in a 3 mm metal sheet bended.

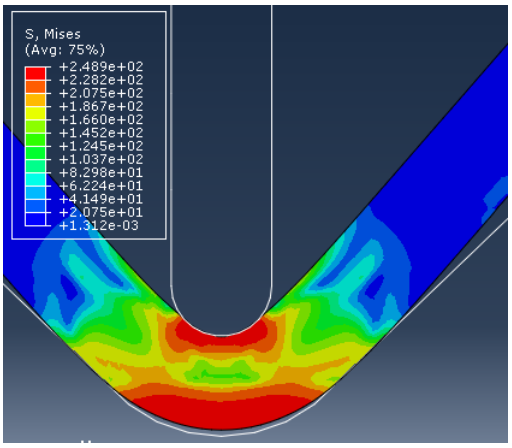

Figure 13 – Stress distribution in a 4 mm metal sheet bended.

It can be verified that most of the force is concentrated in the central bending region of the aluminium sheet. This allowed the mesh to be refined only in this central area of main interest in this work, giving more efficiency to data processing, as the computer present fewer results on the edges of the plates, which are of less interest for this study. These edges would only have greater importance if the *springback* effect, presented in (TRZEPIECINSK; LEMU, 2017), was measured when the punch returned to its initial position after the bending

process was finished.

Table 3 presents the theoretical results obtained from the equation shown in section 2.2, which was obtained from (KALPAKJIAN; SCHMID, 2006). In this table, one can see that all analytical forces calculated using the equation were smaller than the forces proposed by the simulation.

Table 3 – Forces applied to bend metal sheets - numerical and analytical.

Metal Sheet Thickness $[mm]$	Maximum Numerical Force $[N]$	Maximum Analytical Force $[N]$
1	11266	2089
2	20648	8357
3	35484	18803
4	48294	33427

Source: (KALPAKJIAN; SCHMID, 2006)

Table 3 presented very different results from those found using the finite element simulation, as exposed in Figure 14, which compares the results using the simulation (in orange) with those using analytical equation (in blue).

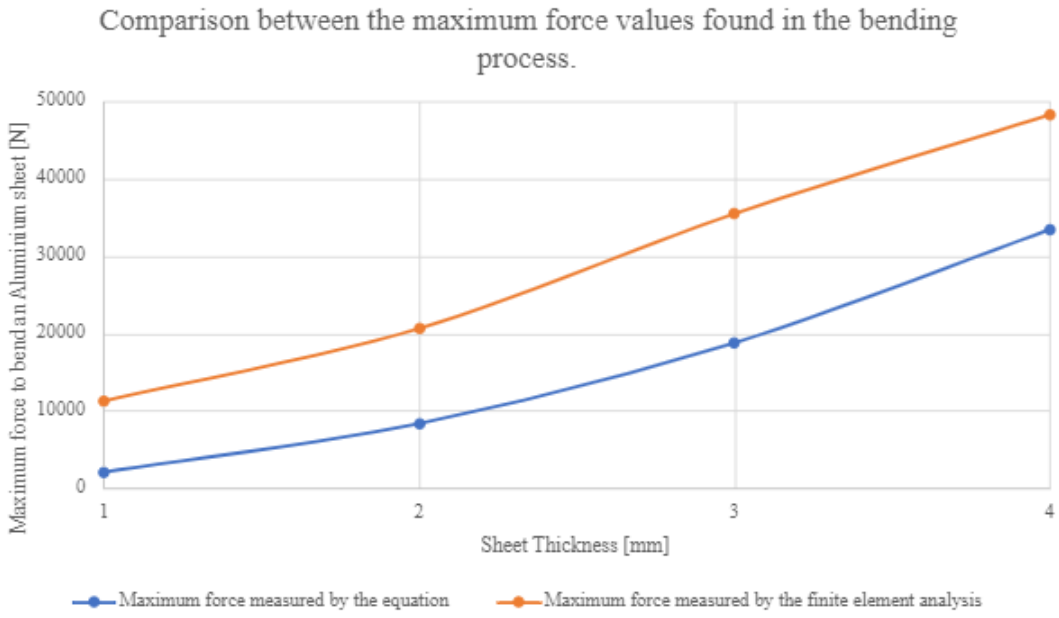

Figure 14 – Graph comparing forces calculated numerically and analytically.

When the thickness of 1 mm is compared, the value calculated for the simulation was approximately 6 times greater than the value from the equation. However, the difference between the value calculated by the equation and by the finite element simulation for the thickness of 4 mm was less than 30% of the value calculated in the simulation.

It is important to note that the graphs shown in Figure 14 follow the same trend but with some differences. The search to determine the reason of these differences can be

considered in a future work on the issue by the improvement of the finite element analysis' use.

The results provided by the numerical finite element simulations were chosen as parameters to determine the maximum bending forces, as they presented higher forces and more accurate data in respect to results of the analytical equation. These simulations identified the load necessary to bend the thickest sheet, considering the actuator limitation. According to these simulations, the maximum load withstand by the device would a 4,93 tons.

It is worth to mention that these tests were subject to an implicit simulation. The result was a load of 4,78 tons, not far from the value found in implicitly analysis, when the sheet bending was subject to an explicit simulation at speeds of 1 mm/s and of 10 mm/s.

4.2.2 Chassis' Sizing

After simulating the sheet bending and identifying the required forces, the chassis was assembled and implicitly simulated in the Abaqus software to determine how much of its structure would deform if subjected to a maximum load of 5 tons with the determined geometry. It is close to 4,93 tons, the maximum load that the device could withstand, accordingly to the implicit simulation.

Each one of the two rectangular plates of the chassis has the following dimensions: 20 mm high, 300 mm wide, and 100 mm deep. Both are connected by four circular cross-section bars, each with a radius of 7,5 mm and a height of 212 mm, perpendicular to the plates, and fixed near the chassis' internal vertices. The design of the bars considered the mould height, the sheet thickness and the punch attached to the actuator, since the bending event is going to occur inside the chassis, between the upper and the lower plate.

To the simulation process, each plate was meshed-up with 4800 *quad* elements and each bar with 6572 *quad* elements. Considering the structure of two plates and four bars, this first series of simulations, used 35888 *quad-type* elements.

The first digital version of the chassis was then available. It was possible to simulate a load applied in the structure Figure 15 and the deformation of the upper plate when the load was applied Figure 16. Moreover, Figure 17 and Figure 18 illustrate the distributions of von Mises stresses in the cylindrical bars and in the upper plate, respectively.

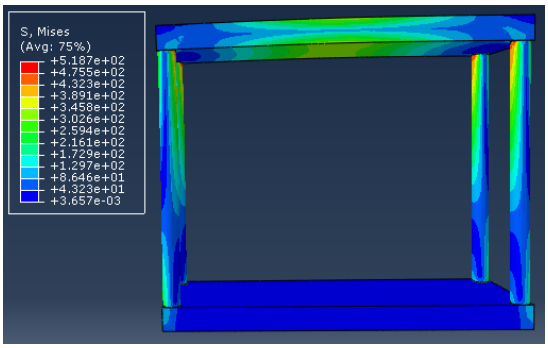

Figure 15 – Chassis 1.0 version, simple structure.

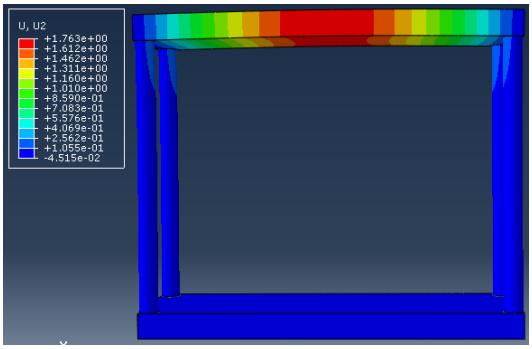

Figure 16 – Vertical displacement in upper plate.

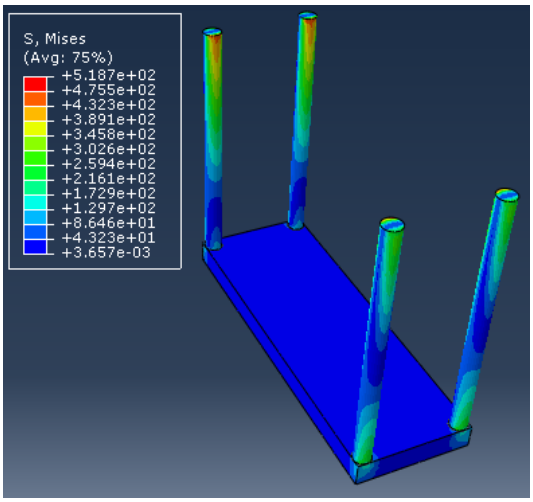

Figure 17 – Circular cross-section bars' stress distribution.

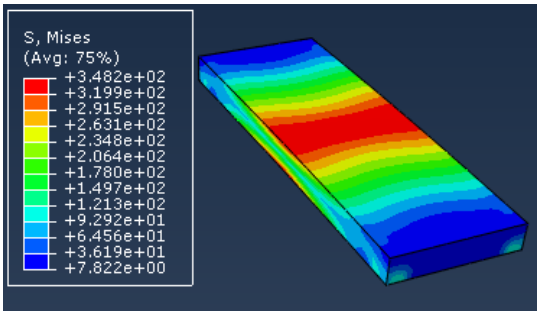

Figure 18 – Upper plate's stress distribution.

During this simulation, considered as the 1.0 version of the project, and given that the punch displacement was 10 mm in the vertical direction, it was initially observed a significant deformation on the superior plate, a displacement of 1,73 mm in the vertical axis. In addition, the highest stress identified was in the bars near the upper plates, at 518,9 MPa.

Since it was possible to notice that the deformation of the chassis was excessively high, to mitigate the problem it was proposed a perpendicular plate-support placed on the upper plate to improve its stiffness, as shown in Figure 19. The final displacement suffered by the upper plate with the support is exhibited in Figure 20. This second simulation is considered the 2.0 version of the project.

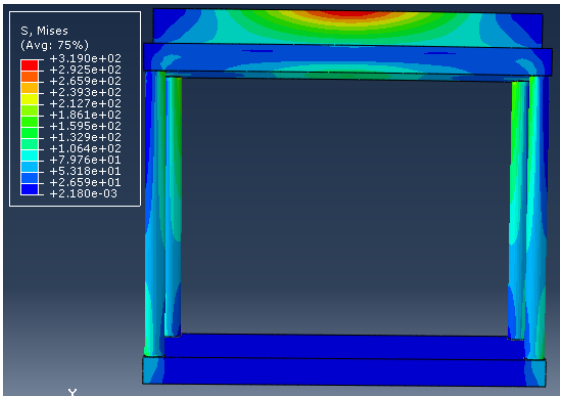

Figure 19 – Chassis 2.0 version

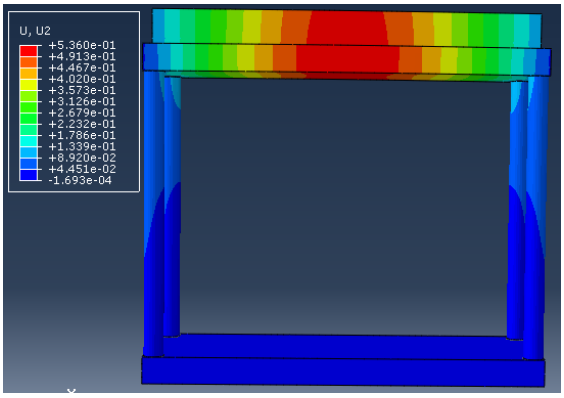

Figure 20 – Vertical displacement in upper plate.

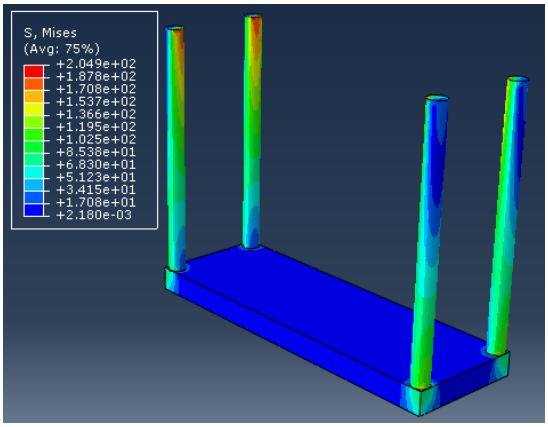

Figure 21 – Circular cross-section bars' stress distribution.

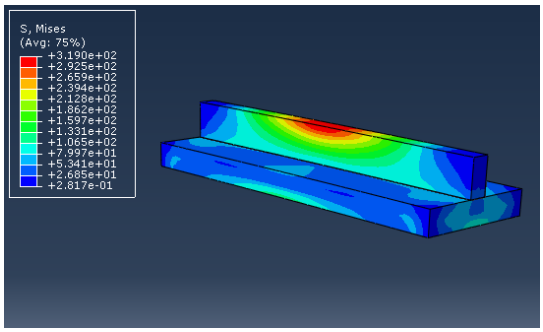

Figure 22 – Upper plate's stress distribution.

The support was a rectangular-shaped plate with the following dimensions for the 2.0 version simulation: 300 mm in length, 15 mm in height, and 20 mm in depth, as shown in Figure 22. To this simulation, the support was meshed-up with 3900 *quad* elements.

An important consequence that deserves to be emphasized is that the area subject to the maximum stress in 2.0 version simulation was the upper support instead of the bars near the upper plates, observed during the 1.0 version simulation (since it is possible to compare Figure 19 with Figure 21 and Figure 22). Therefore, 2.0 version presents a considerable improvement when compared to the initial simulation. The highest stress identified was lowered to 319,0 MPa and the upper plate vertical displacement to 0,54 mm.

The project could still be improved by increasing the height of the upper support from 15 mm to 50 mm, as shown in Figure 23 and Figure 24. This modification, considered the 3.0 version, also increased the support digital mesh to 4875 *quad* elements. In this simulation, the highest stress was lowered to 178,0 MPa and the upper plate vertical displacement to 0,32 mm.

The 3.0 version showed that the edges of the support had low von Mises stress when compared to its central area. Thus, to reduce the weight of the external structure of the

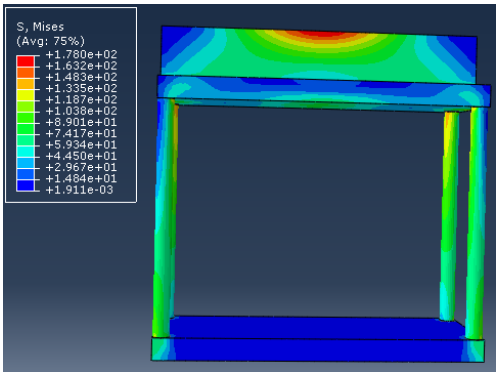

Figure 23 – Von Mises stress applied in the 3.0 version chassis' version of the project.

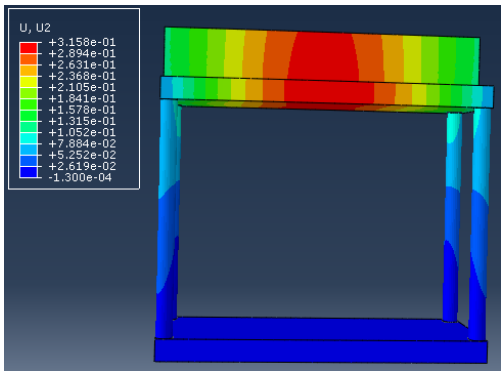

Figure 24 – Vertical displacement in upper plate.

bending machine, its size and the costs related to manufacturing material, it was considered that the support could have two diagonal small cuts on the sides of it attached to the top, making the support-plate looking like a trapezoid when viewed from the front. Thus, this new chassis design is considered the 4.0 version of the project and is exposed in Figure 25. Because of this size reduction, this version presented a decrease in its support digital mesh to 4464 *quad* elements.

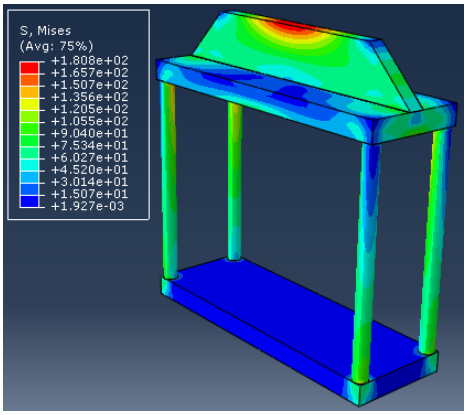

Figure 25 – Von Mises stress applied in the 4.0 version chassis' version of the project.

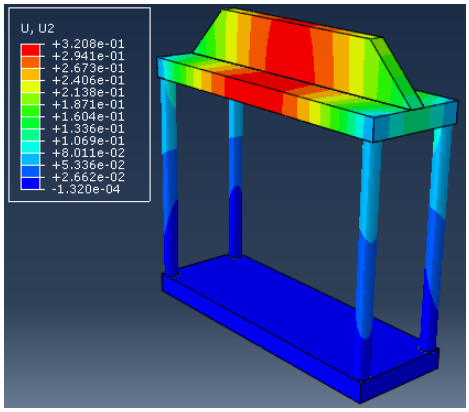

Figure 26 – Vertical displacement in upper plate.

The highest von Mises stress for the 4.0 version was concentrated in the central and in the upper region of the trapezoidal support consisting of 180,8 MPa, an irrelevant increase in respect to the 3.0 version. The maximum vertical displacement was 0,32, the same of 3.0 version.

Finally, after optimizing the design with the final maximum von Mises stress, it was verified that SAE 1020 steel, a commonly used metal alloy, could be used to make the chassis, considering it cost-benefit relationship.

4.2.3 Punch's Sizing and a Brief Mould Analysis

After defining the external structure, a new simulation was carried out to verify the punch's best size, as it has the risk of buckling when a strong load is placed on it. This failure could, besides ruining the manufacturing process of bending a sheet, damage the external structure, since the actuator would receive a reaction force perpendicular to its main axis.

A 50 mm punch was initially simulated, with vertical displacement, following the project's initial idea. *quad-type* elements were used with mesh refinement near the lower end of it, resulting in a mesh with 1462 elements. Once this simulation was completed, it was possible to verify that the punch suffered a displacement of 0,034 mm horizontally at the lower end compared to the initial position on the x-axis, as shown in Figure 27. This small value does not bring a significant buckling risk.

In addition, the average von Mises stress in the punch, shown in Figure 28, is 110 MPa and the maximum is 899 MPa at its base, as shown in Figure 29). This remarkable difference was expected since the tip of the punch is in constant contact with the metal during the bending process. To outcome the limitations related to acquiring a material with a significant yield stress around 900 MPa, it is suggested to heat treat the tip of the punch during the punch manufacturing. The heat treatment will increase the rigidity of the punch tip in such a way that it will not easily be wasted during the metal sheet bending processes.

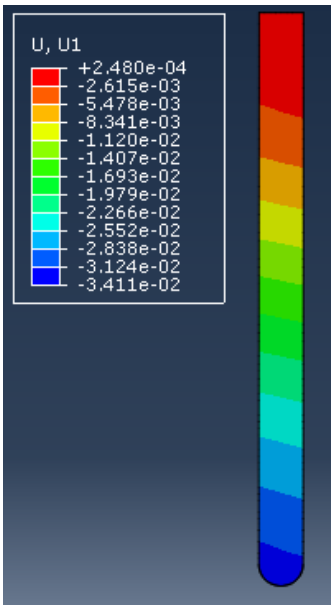

Figure 27 – Horizontal displacement in the 50 mm punch.

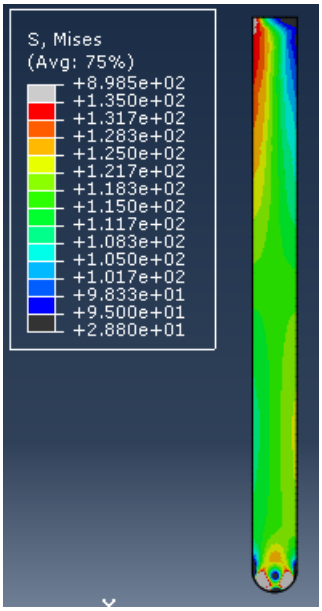

Figure 28 – Von Mises stress in the 50 mm punch.

An additional simulation was done for a punch of 30 mm height, maintaining the other dimensions, since the risk of buckling would be lower, and less material would be used to build the punch. In this case, the mesh resulted in 1246 *quad* elements, lower than the 1462 elements used in the punch of 50 mm height. The maximum horizontal displacement

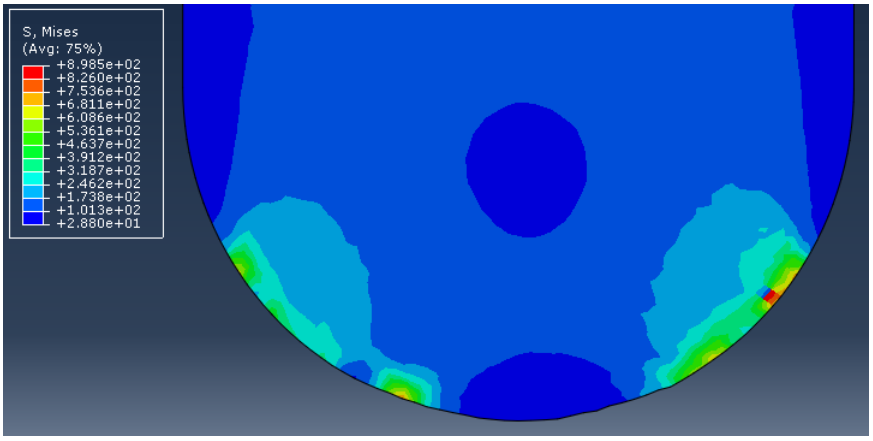

Figure 29 – Von Mises stress in the 50 mm punch (amplified figure).

measured was 0,0045 mm, around 13% of the displacement identified on the 50 mm punch, as shown in Figure 30. It is valid that there was no significant difference in the average von Mises stress along the punch, and the average von Mises stress for the 30 mm punch was 105 MPa. Figure 31 and Figure 32 show the results of the simulations.

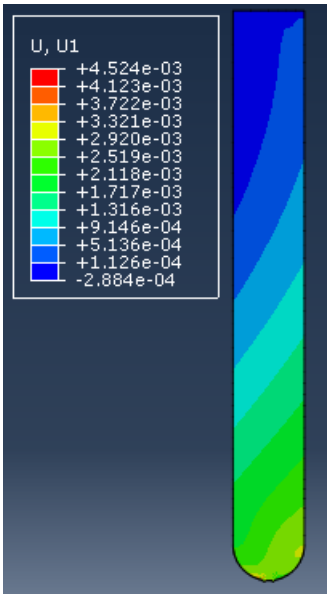

Figure 30 – Horizontal displacement in the 30 mm punch.

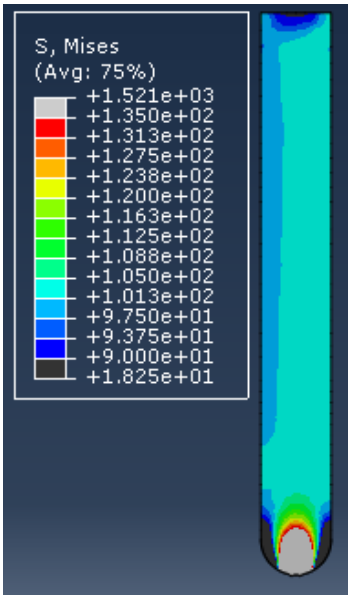

Figure 31 – Von Mises stress in the 30 mm punch.

The punch chosen for the project was the 30 mm one, as its stress is very close when compared to the 50 mm punch. It is smaller and it has a reduced buckling risk. As mentioned, a heat treatment will be carried out on the punch's tip to improve its rigidity and reduce failure incidence on it.

Finally, during the mould simulation (shown in Figure 33), it was noticed that it did not present high von Mises stresses as the punch did. The highest stress measured by the mesh with 1184 *quad-type* elements refined at the mould's "V"-die vertices was 107,1 MPa, at the end of the bending process of a 4 mm thick aluminium sheet. In conclusion, a SAE

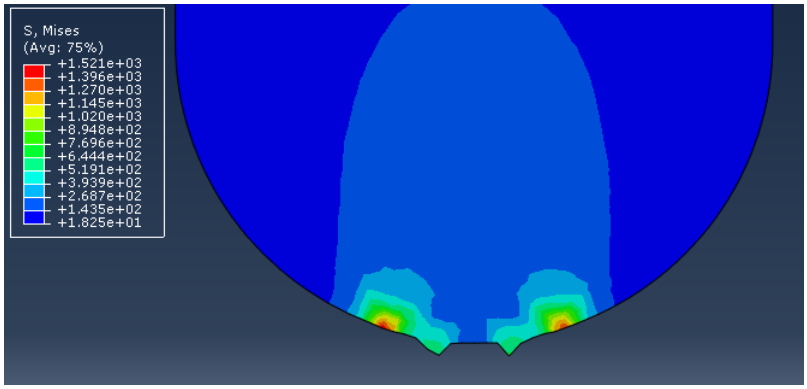

Figure 32 – Von Mises stress in the 30 mm punch (amplified figure).

1020 steel supports the applied stress both in the punch and the mould.

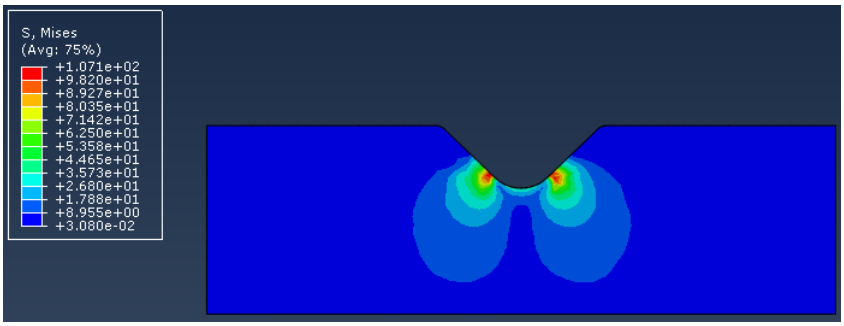

Figure 33 – Finite Element Analysis of the Mould, maximum stress of 107 MPa.

4.3 The Result of the Project's Design and Sizing in Abaqus

An idealization of the device is shown in Figure 34. It shows how the chassis, the mould, and the actuator would be arranged. Once all parts were designed, this "V"-bend process or three-point bending can be compared with (HINCHY et al., 2020).

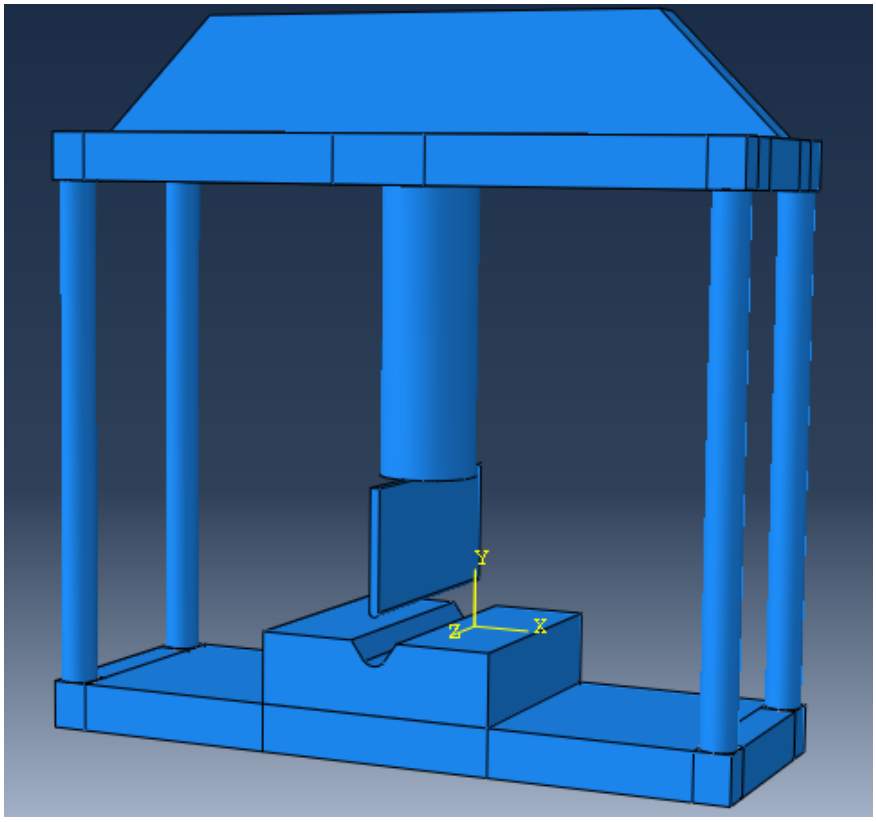

Figure 34 – Bending Machine Model (if improved, one could call it a digital twin of the physical project) developed in Abaqus software.

In the case of a more complete simulation, analysing more mechanical components and evaluating each of them over a period, the simulation of the metal sheet bending machine could lead to a digital twin of the project. As mentioned before, digital twin is a digital representation of a physical system, as shown in (ÖZEN et al., 2021), (EDER; CHEN, 2020) and (BLOMFORS; LUNDGREN; ZANDI, 2020).

The device design and the finite element simulations are concluded, checking the maximum stresses in each mechanical component of the project and the average stresses along the punch. During the finite element simulations, the vertical displacements of the chassis and the horizontal rearrangement of the punch were measured. With the values simulated, the next step is the device manufacturing, presenting the assembly process of the machine.

5 Device Manufacturing

The SAE 1020 steel parts were previously dimensioned and demanded into separate pieces. This material was submitted to an oxy-fuel cutting to the dimensions specified by the technical drawings mentioned in Appendix A, as the example shown in Figure 35 (physical model used for the top and bottom plates). Additionally, Figure 35 presents only one plate, because both the upper and the lower plate have the same dimensions, only one of them was represented. One can say that the punch, the other plate, and the trapezoidal support were in the same external condition (with burrs and with iron oxide). The material was subject to machining and welding processes in the SG-9 Laboratory to ensure that the pieces would fit together.

Figure 35 – Plate physical model before any machining.

Furthermore, the bars were obtained in that laboratory, as detailed in subsection 5.1.4. Their dimensions are 19 mm in diameter and 217 mm in height, according to the model illustrated in Figure 36.

These parts were purchased in SAE 1020 steel, as proposed in the previous chapter and they were machined. Except in the case of the punch and of the mould, they were also welded.

Figure 36 – cutted bar physical model.

5.1 Chassis Machining

This section will show the steps involved in machining the chassis, starting with removing burrs and iron oxide. After removing the residual material from the oxyfuel cutting, a small undercut was machined in the centre of the lower plate using a milling machine, where the mould will be coupled and can be easily changed. After that, holes were made for fixing the bars and an additional hole was made in the centre of the upper plate to help fixing the actuator. Furthermore, a description will be made of how the bars manufacturing was carried out.

5.1.1 Deburring and Iron Oxide Removal from both Plates and Support

It was noticed that the parts had many lateral imperfections, burrs, and had iron oxide on the upper and lower parts of each piece, as shown in Figure 35. These imperfections in the material are commonly found in metals after they suffer an oxy-fuel cut. Therefore, the use of a grinder was proposed to remove the burrs. Thus, with assistance of technicians from UnB, the plates were ground at their edges. Figure 37 shows an image captured during this process, made with a Delta Rockwell model 23 – 226 "7" grinder, at 2850 rpm.

Figure 37 – Plate grinding.

Figure 35 and Figure 38 can be compared to verify the difference between the plates before and after the removal of burrs (still with oxidized iron), respectively. Similarly, it is possible to show the same process for the trapezoidal support, which had burrs that were grounded, as can be seen when comparing images Figure 39 and Figure 40.

Figure 38 – Plate with iron oxide but without burrs.

Figure 39 – Trapezoidal support with iron oxide and burrs.

Figure 40 – Trapezoidal support with iron oxide but without burrs.

Once the burrs were removed, as shown in Figure 38 and Figure 40, the removal of iron oxide from the steel on the plates and support was done, as shown in Figure 41 and in Figure 42, the first one representing the process made on the lower plate and the second one on the support.

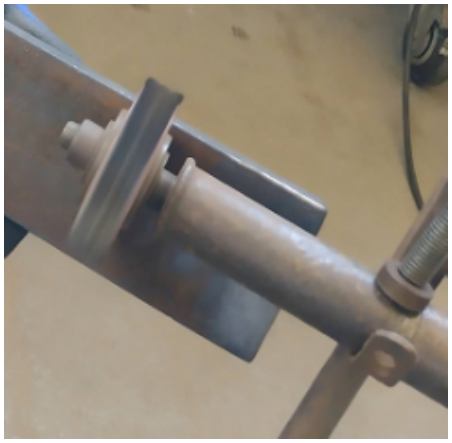

Figure 41 – Plate's iron oxide removal process.

Figure 42 – Support's iron oxide removal process.

UnB also provided the necessary equipment to remove the iron oxide - with the rotating steel brush connected to a motor. The iron oxide removal process was done using a Jowa's S/A machine with a three-phase asynchronous motor that could have 380 V in the star connection and 220 V in the delta connection. The motor speed variation was from 2800 rpm to 3400 rpm. Also, with the assistance from UnB technicians, the iron oxide removal process was completed for the plates and the trapezoidal support, with the main result shown in Figure 43.

Figure 43 – Support and Plates without burrs and iron oxide.

5.1.2 Milling Process in the Lower Plate

Once the plates were free of burrs and iron oxide, the milling process of the lower plate was carried out using the SG-9 Laboratory milling machine. To do this, under the instruction and supervision of a technician, the plate was initially fixed to the machine table. Once the plate has been firmed and the machine was ready, the process of removing material layers began, as shown in Figure 44. The milling cutter used in this process was a Mez Mohelnice Národní Podnik machine, with voltage variation between 380 and 220 V for the star and delta connections, respectively. In addition, the milling cutter used its maximum rotation speed of 1740 rpm for this manufacturing process.

Initially there were four steps through the milling process, each with an approximate advance of 56 mm/min and a removal of 0,5 mm of material at each complete step. As a result, an undercut of 2 mm was made in the inferior plate with the milling cutter. It is important to note that the diameter of the milling cutter used was 25 mm. From this point on, since the recess was exactly 100 mm, three more steps were made with the machine's advance reduced by half (28 mm/min) so that the mould could be perfectly fitted into the lower plate. Moreover, during the last three steps, 2 mm of material was directly removed in each step.

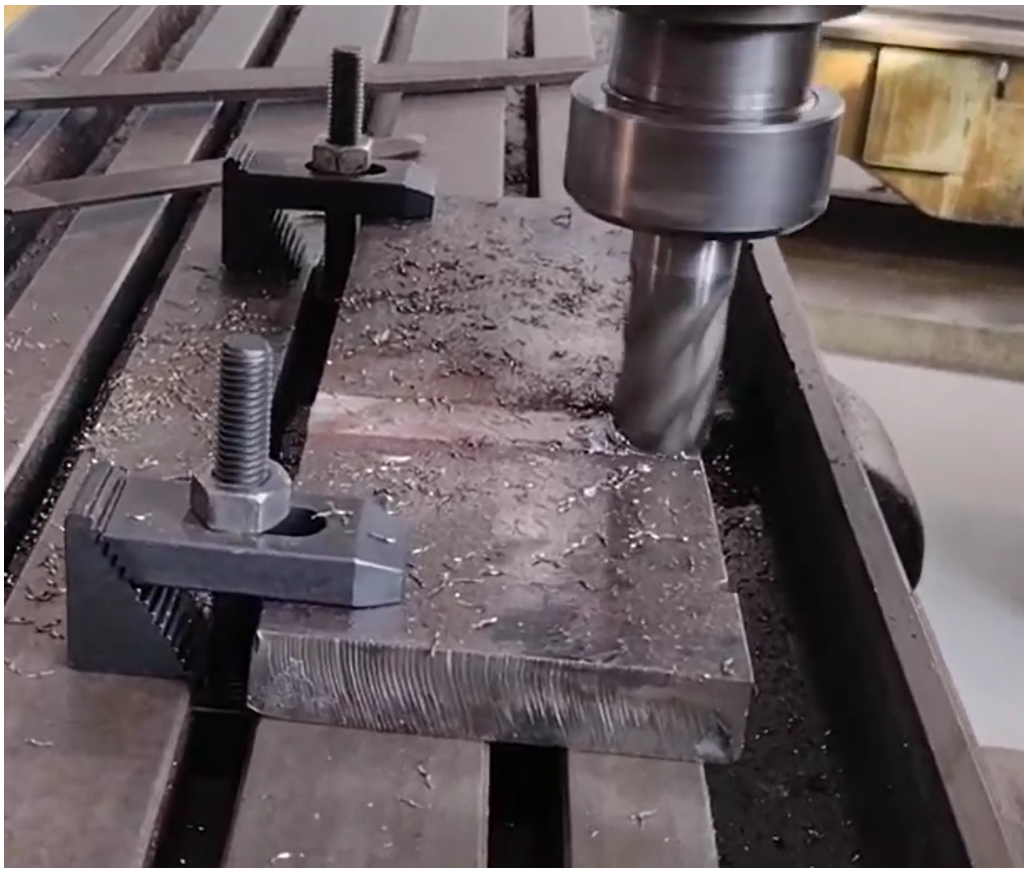

Figure 44 – Milling process cutting the inferior plate.

At the end of the milling process, Table 4 was created, showing the values of cutting speed, feed rate, effective cutting speed, and the material removal rate, using the equations mentioned in (ÁVILA, 2022) and (BARRETO, 2022).

Table 4 – Data about the milling process

Parameter	Calculated Value
Rotations per minute (RPM)	1740 rpm
Cutting Speed (V_C)	0,1367 m/min
Minimum Forward Speed (V_{fmin})	0,04872 m/min
Maximum Forward Speed (V_{fmax})	0,09744 m/min
Maximum Effective Cutting Speed (V_{ECmin})	0,1451 m/min
Maximum Effective Cutting Speed (V_{ECmax})	0,1678 m/min
Minimum Removal Rate (Q_{Mmin})	0,609 cm^3/min
Maximum Removal Rate (Q_{Mmax})	1,218 cm^3/min

Source: (BARRETO, 2022) e (ÁVILA, 2022)

During the milling process, the tool was cooled with cutting fluid, also available in the SG-9 Laboratory. The cutting fluid data, such as density, cutting depth, and colour, are shown in Table 6, in Appendix B. While the inferior plate was being machined, the liquid was poured over the cutting region.

5.1.3 The Process of Drilling the Plates

After the bottom plate was milled, it was marked with the aid of a paper jig, in relation to the undercut made, at a distance of 84 mm and, in relation to the larger end, 10 mm, so that it would be the centre of the hole that would serve as a guide for drilling the hole with a 6 mm diameter bit. Figure 45 shows the first result of the drilling process, the initial hole that serves as a guide for the larger hole. The holes in both plates (both in the lower and upper ones) were drilled with the same 17 mm diameter bit.

The dimensions of the recess in the bottom plate were also marked on the upper plate to ensure that when the upper plate was marked to make the guide hole. Once the guide hole was done, the drill tool was changed to a 17 mm diameter one. As a consequence, the hole on the plate would be made with the same dimensions as the bottom plate.

The drilling machine used in this process was a Boice Crane Strands S53 with AC supply voltage of 220 V, 60Hz and with a rotation variation of 1700 to 3450 rpm.

The result of the mentioned drilling process was eight 2 mm depth holes (Figure 46). Since the machining process leaves some burrs on the surface of the piece, once these holes were completed, the remaining burrs were removed with a file also available in the

Figure 45 – Inferior plate after the 6 mm diameter hole drilled.

Figure 46 – Inferior plate after the 17 mm diameter holes drilled.

SG-9 Laboratory. Figure 47 shows how the situation before the removal of these burrs and Figure 48 exhibit the result after the burrs were removed with a file.

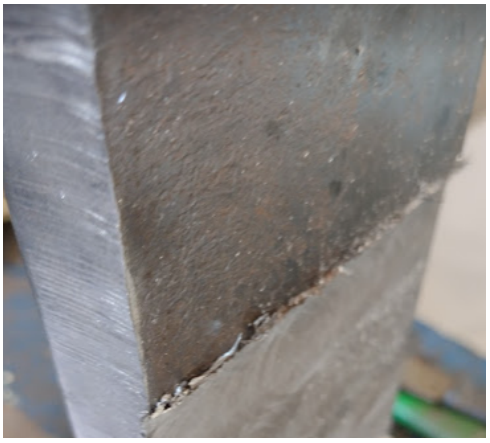

Figure 47 – Lower plate after machining process, presents burrs.

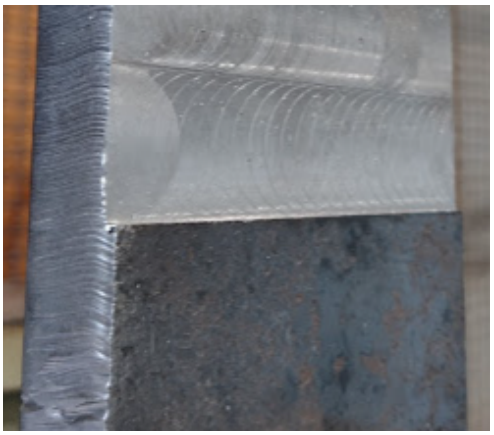

Figure 48 – Lower plate after the file burr removal.

Additionally, a hole with a diameter of 9 mm was made in the centre of the upper plate to allow the use of a screw to hold the actuator, as seen in (ENERPAC, 2022). The recess depth was 6 mm since it is a hole where a screw will be attached. Figure 49 shows the location and process in which the hole was made in the upper plate.

With the completion of the subtractive manufacturing process of the plates, it was possible to start the manufacturing of the bars, since these would guarantee the support of the plates and it would be possible to join the parts and form the chassis.

Figure 49 – Drilling superior's plate middle hole.

5.1.4 Bars Machining

The bars were initially cut from a larger bar. The cut was made using a Makita Maktec circular saw machine available in SG-9 Laboratory, as shown in Figure 50. This disc had a rotation speed of 4000 rpm, with a saw blade diameter of 260 mm, as presented in (MAKITA, 2022). The bars had a diameter of 19 mm, slightly larger than proposed during the simulations, but they were used to facilitate the reuse of materials from other projects and to reduce costs. The bars were cut to a length of 217 mm (a bit more than the expected value of 212 mm previously mentioned in the last chapter), as they still needed to be machined and some material was removed.

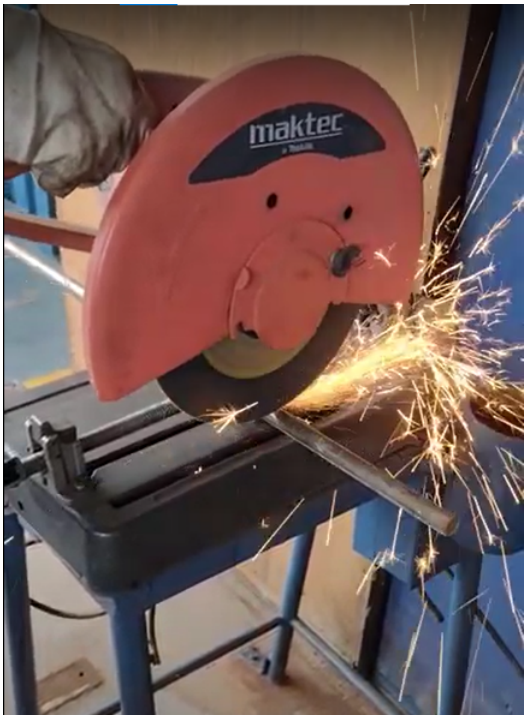

Figure 50 – Bar being cut which will generate the smaller bars with 217 mm to support the chassis.

Once the bars were cut with their original 19 mm diameter, they needed to be machined on a lathe to be fitted into 17 mm holes. Thus, Figure 51 exposes the bar being machined on the SG-9's mechanical lathe.

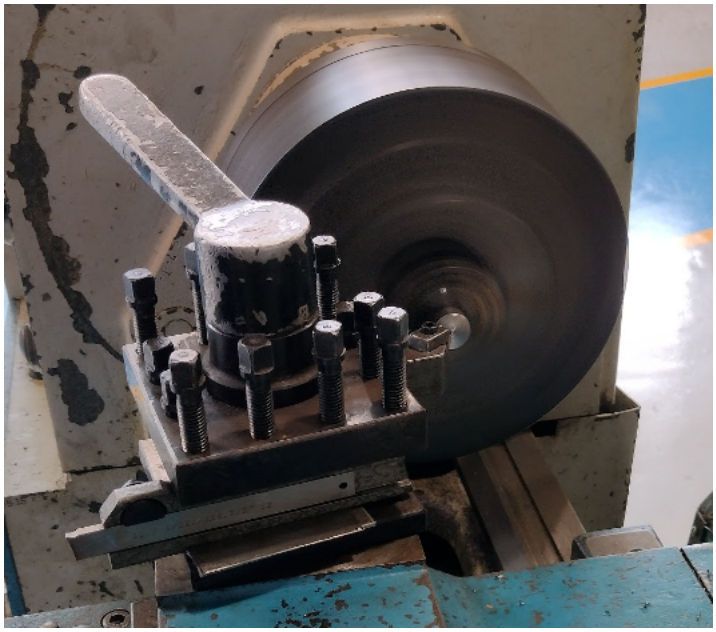

Figure 51 – Bar lathe machining.

The lathe used to both face and step of the bars was the Engemaq Imor RN400, working at 450 rpm and with the feed rate controlled by a technician. Due to this manual turning, it was not possible to calculate values such as the feed rate, the cutting speed, and the chip removal rate as shown in (BARRETO, 2022) and (ÁVILA, 2022).

Figure 52 – 217 mm bar after lathe machining with lower size dimensions in its borders.

When the lathe machining part of the bars was completed, as seen in Figure 52, they fit into the plates and had the same height. Given the result of the completion of the bars machining process, the next section (section 5.2) will show the manufactured mould.

5.2 Mould's Manufacturing Process and the Assembly Preview

The CNC milling machine was used to create the recess in the project's mould. This allowed the production of the "V" recess removing material from the mould and ensuring a three-point bending process. Moreover, a cutting fluid was used to help the milling process, which provided a better workmanship to the machining process of the recess, as shown in Figure 53.

Figure 53 – CNC Milling Process to machine the mould.

The result of the CNC milling was revealed in Figure 54 and Figure 55. It is possible to see the workmanship of the mould and the recess that is in accordance with what had been planned in the technical drawings shown in Appendix A.

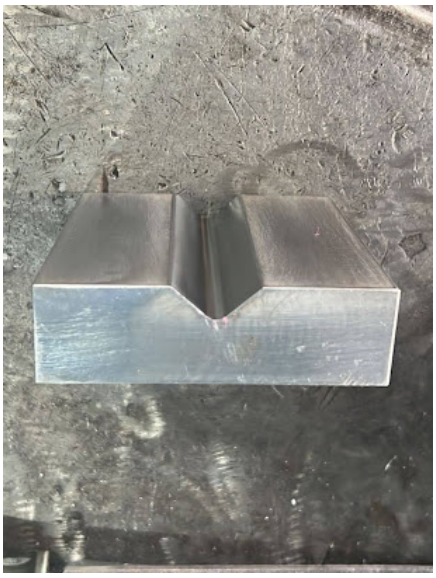

Figure 54 – Already machined mould's frontal view.

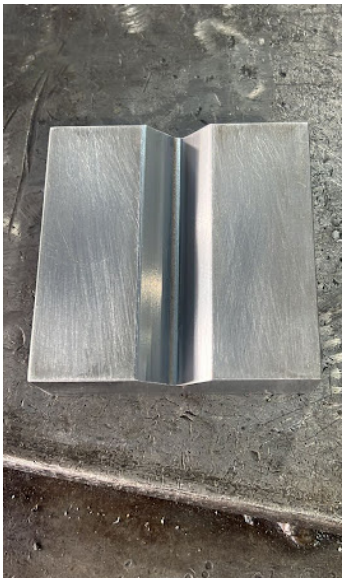

Figure 55 – Already machined mould's superior view.

The physical chassis model was assembled when the mould became available. It was verified that the recess made in the chassis was in accordance with the 100 mm of the mould. The fit was perfect, as shown in Figure 56. As result, there is already an idea of what the physical twin of the project would look like.

Figure 56 shows the pieces fitted in the process. The image can be compared to Figure 34, in which it is possible to perceive the bars attached to the plates, the mould centred on the lower plate, the trapezoidal support above the upper plate, with only the actuator and punch missing in the image.

The recess was made in such a way that even other moulds can be placed, confirming the possibility of other types of bends, considering the maximum bending load for the 5 ton actuator.

Figure 56 – Chassis assembled by fitting its mechanical components.

It is important to note that the iron oxide removal process left the material with a new appearance. Additionally, oil was applied to the surface of the parts with the intention of avoiding short-term oxidation in the device.

5.3 Welding Process

Once the bars were ready and fit into the holes made in the plates, it was possible to start the welding process of the plates with the bars. Metal inert gas (MIG) welding was used to make the weld points, as already mentioned in section 2.6, because it is a type of welding with low cleaning needs after application. Thus, Figure 57 shows the weld points applied to join the plates with the bars. During the welding process, the bars were checked for straightness with the aid of a metal square.

A second welding was carried out at the junction of the plates with the bars, with the result of this second process shown in Figure 58. However, in this second time, the parts

Figure 57 – MIG weld point applied between the plates and the bars.

Figure 58 – Coated electrode weld applied between the plates and the bars.

were welded with a coated electrode through an electric arc, present in the SG-9 Laboratory. The electrode used for this part was an E6013 and once the weld was made, it could not be undone, and when completed, the weld area was brushed to clean it.

This section and other previous sections detailed all the manufacturing work developed in this project. The next section describes additional manufacturing activities.

5.4 What Should be Done in Order to Complete this Work

Some tasks still need to be completed to finish this project. A rounding would be made on the punch tip to transform it in a semi-cylinder with a radius of 2 mm, as already simulated and detailed in section 4.1. Once the machining of the mould piece for the punch is completed, it will be submitted to a heat treatment described in subsection 4.2.3, followed by the coupling of the punch to the RC-51 actuator. The attachment of the RC-51 actuator on the punch would be done through a fitting or a rubber connector. Thus, all that is left is to place the actuator in the centre of the upper plate of the chassis and align it. This would be done by inserting a pin or a screw between the actuator and the hole in the centre of the upper plate of the chassis, which is exposed in Figure 49, and checking if the punch is parallel to the "V"-die.

Therefore, when the device is ready it will be possible to create its control system, represented by a sensor in order to show the measured force.

6 Device's Control System

This chapter will show how the device control system will be implemented through the Arduino IDE, since there are no electromechanical actuators and only the sensor output could be changed. The control system is materialized by an Arduino board device and its components: the Wheatstone bridge (HX711 component), the strain gauge (sensor to measure the force according to the load that will be applied by varying the resistance of its internal wires) and some wires to connect the electronic parts.

It is interesting to mention that electronic devices operate in direct current mode and maximum voltage of 5 V, as seen in Table 7. Therefore, the equipment is not at risk of getting burned or giving human-fatal electrical shocks. The Arduino circuit board was chosen because it is a didactic device, it is easy to handle, it has a series of sensors which easier to acquire when compared to a Raspberry Pi, and it is cheaper than a field programmable gate arrays (FPGA) interface.

6.1 Electronic Device Assembly

Initially, the strain gauge, shown in Figure 59, was attached to the punch, since it is under conditions of elastic regime and its surface (where the strain gauge will be connected) is going to be polished. Thus, the compressive force, which is applied to the punch by the actuator and the metal plate that is being bent, generates an elastic deformation in the punch itself. As a consequence, the strain gauge measurement varies, since the resistance of the strain gauge changes according to how much it is deformed, as verified in (BENTLEY, 2005).

Thus, the strain gauge is connected to the HX711 board (Figure 60), as shown in Figure 62, so that $A+$ and $A-$ are connected to the strain gauge wires. The HX711 board is connected to the Arduino (Figure 61) with a voltage of 5 V and grounded on the "GND" pin (ground pin). The outputs $A1$ and $A2$ respectively present the components DT ("Digital Output") and SCK ("Serial Clock"), as shown in the datasheet in (AVIA, 2022).

It is important to mention that some changes may occur to improve the equipment's performance and organization, such as soldering the strain gauge connector wires with the HX711 board and those that depart from it arriving at the Arduino device.

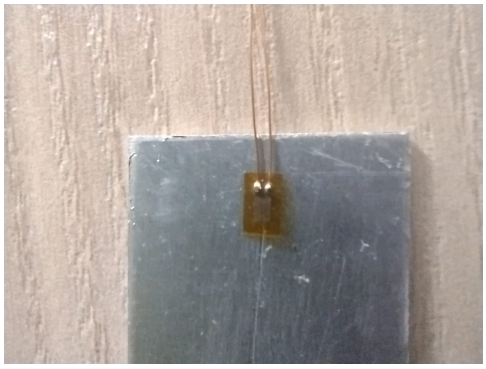

Figure 59 – Strain gauge model and how it would be attached to the punch.

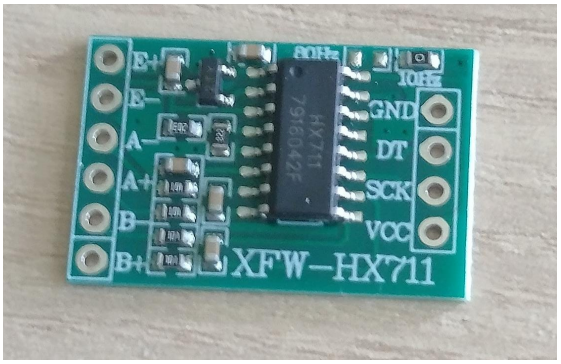

Figure 60 – HX711 board showing its inputs and outputs.

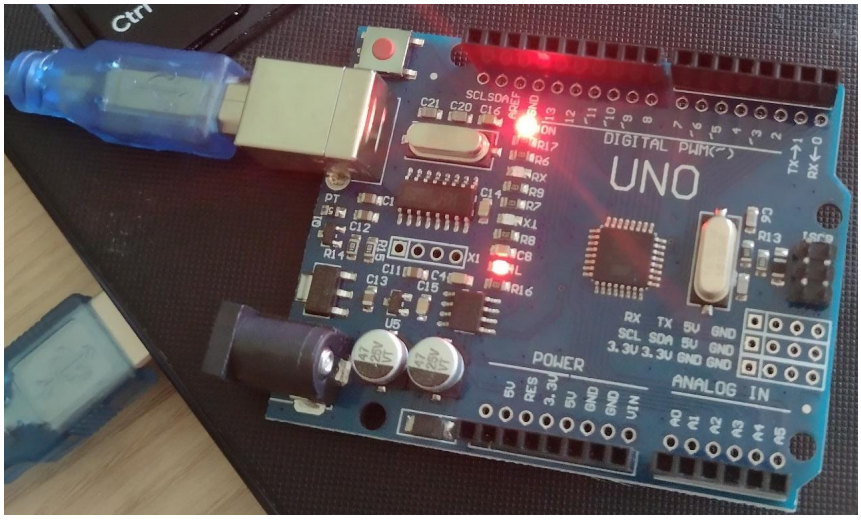

Figure 61 – Arduino Model.

Figure 62 and Figure 63 show how the Arduino connects to the equipment through the strain gauge, to the HX711 board, and to the connector wires. The $A+$ and $A-$ ports of the HX711 board were chosen because they have a maximum error of 40 mV (when compared to the $B+$ and $B-$ input, which has a maximum error of 80 mV), as shown in (AVIA, 2022).

Moreover, small bending machines performing tests require sensors with high precision. The use of more precise and efficient sensors is being developed, as shown in (ARAROMI et al., 2020). Hence, the use of high precision sensors was mandatory, considering the use of small-scale metal sheets (100x100x4mm).

Finally, for those who want to specialize in the field of electrical materials and their applications in the use of strain gauges and Wheatstone bridges, it is possible to implement a strain gauge with a resistance made of another material to measure the force applied to the punch, as presented in (MADSEN et al., 2016).

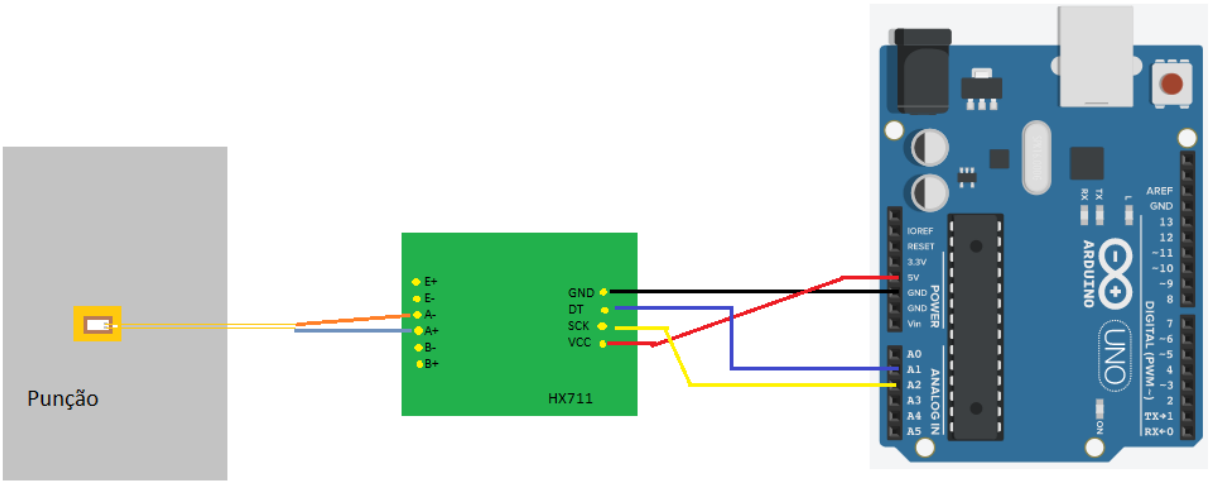

Figure 62 – Schematic drawing exhibiting how Arduino's device should be attached to the punch.

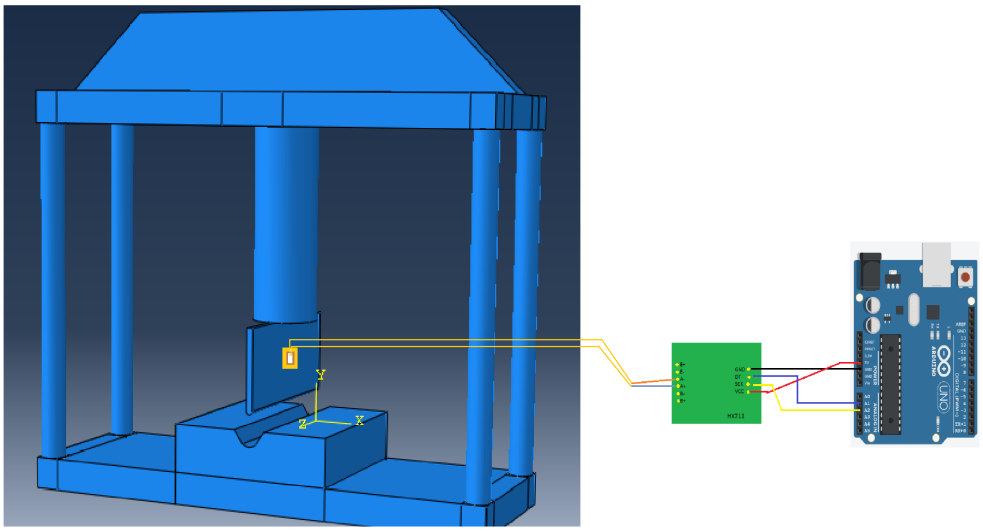

Figure 63 – Schematic drawing illustrating how Arduino's device should be connected with the project.

6.2 Force Monitoring

Since the actuator will provide a force on the punch and it will undergo elastic deformation, the strain gauge will record how much the punch was deformed. Initially, this strain gauge has a resistance of, approximately, 120 Ω, as seen in (OMEGA, 2023). Thus, the force variation in the system can be measured.

According to (INSTRUMENTS, 2022), the force can be measured by checking the voltage between the strain gauge in its initial and final states, as shown in the equation below, where ϵ represents the strain, V the measured electrical voltage, and R the varying resistance.

$$\epsilon = \frac{V_{deformed} - V_{not-deformed}}{GF \cdot Vcc} \tag{6.1}$$

In this part, the value of *GF* is given as the *Gauge Factor*, found in other articles, such as (MADSEN et al., 2016).

$$GF = \frac{\Delta R/R}{\epsilon} \tag{6.2}$$

Once the force data is monitored, the Arduino system will output a signal that will be compiled in the computer and that will follow a code to be executed. Finally, with the compiled code, the algorithm will process the data received by the Arduino.

It is worth mentioning that force measurement would be given by an equation with a transfer function $P(s)$ in the "s" domain, after the Laplace Transform, as seen in (BANKO, 2012):

$$P(s) = \frac{1 - e^{(sT)}}{sT} \tag{6.3}$$

It is worth noting that the variable T is the time for the impulse function to travel through the strain gauge, which can be written as the ratio between the length L of the strain gauge and the propagation velocity ν of the *shockwave* in it.

$$T = \frac{L}{\nu} \tag{6.4}$$

Thus, when the controller project is completed, the transfer function of the physical system already exists. It is important to note that the type of controller to be used has not yet been chosen, as a controller can be modified to facilitate control adjustment.

6.3 The Code Used to Obtain the Force Needed to Bend a Metal Sheet

Once the entire sensing system is ready, it is interesting to mention how the Arduino's device calibration would be performed. For this purpose, the code used was created on Arduino's IDE virtual platform. It is important to mention that since the project is not yet completed, the code cannot be fully calibrated and may require adjustments. However, the code presented was able to capture the variation of load applied on a small aluminium metal plate that served as an initial test. When the strain gauge was fixed on the aluminium plate, different forces were applied. The value collected by the strain gauge increased when the plate was compressed, and it decreased over time since the compression was released.

Therefore, the code can be written in a way that initially the Arduino's input ports $A1$ and $A2$ are connected to the HX711 board's DT and SCK serial ports (following the schematic drawing illustrated in Figure 62). Thus, the code starts by searching for the *offset* value. Once the value is established, the *offset* value will be 0, and from the moment the *void loop()* function starts to execute, new load values will be considered for the measurements. This code was based on the project developed in (USAINFO, 2023).

Code 6.1 – Code used to obtain the force needed to bend a metal sheet

```
#include "HX711.h"

#define DT A1     // A entrada A1 será conectada com a saída DT
#define SCK A2    // A entrada A2 será conectada com a saída SCK

HX711 medida;    // habilita a variável medida com o dispositivo
   HX711

void setup() {
  medida.begin (DT, SCK);     //  Ativa as sáidas DT e SCK do
     programa
  Serial.begin(9600);
  Serial.print("Offset value:  ");
  Serial.println(medida.read());  // Aguarda o término de
     verificação da carga que está sendo aplicada
  medida.set_scale();             // Utiliza uma medida padrão de
     verificação
  medida.tare(20);                // Fixa o a carga inicial como
     offset
  // basicamente a carga inicial será 0;
  Serial.println("And let's go! \n");
}

void loop() {
  Serial.print("Load measured:  ");
  Serial.println(medida.get_value(10),0);  // Retorna a carga
     descontando o offset
  delay(250);
}
```

7 Conclusions

As seen in chapter 4, the project design followed the plan and presented reliable results. It comprised the conceptualization, finite element simulation and a significant portion of the device's manufacturing. Several tests were carried out under different conditions, with metal sheets ranging from 1 mm to 4 mm, with different loads for each bending process. Additionally, a comparison of the forces resulting from the simulation was made with the analytical force calculation shown in (KALPAKJIAN; SCHMID, 2006). Moreover, the chassis, the punch, and the mould were sized, and materials were suggested.

The manufacturing phase of the project presented was seen in chapter 5, showing the machining and undercuts made in the materials. It should be mentioned that the manufacturing part was not fully finished. Furthermore, chapter 6 presented how the equipment control system would be implemented, beginning with a strain gauge attached to the punch and ending with a code to read the punch force.

This work presented a variety of simulations and aims to help students learn in the field of Mechanics of Materials and Manufacturing Processes. It also considers that the device will continue to be manufactured. Finally, the suggestions that will remain for future projects are presented.

7.1 Suggestions for Future Works

The first improvement was already mentioned in chapter 4, when the finite element simulation obtained a different result from the analytical equation presented in (KALPAKJIAN; SCHMID, 2006). For this, it is possible to verify the values considered in the simulations and consider factors not mentioned in this work. It is worth to mention that the trend found in Figure 14 can be maintained and, if possible, improved.

In chapter 4, a bending simulation was performed and it did not consider the bent material *springback* effect, as explained in (TRZEPIECINSK; LEMU, 2017) and in (KALPAKJIAN; SCHMID, 2006). This effect would be important to be analysed since the simulation shown in that chapter does not consider the punch recoiling. Thus, it could be suggested a future work to perform a simulation analysing the *springback* effect and comparing the result obtained with analytical solutions or even other articles.

Besides, for a better arrangement of the project's actuator, it would be interesting to evaluate the possibility of making a hole throughout the top plate and the trapezoidal support with the intention of a better fixing to the project's actuator, since it has a threaded region near the head, as seen in (ENERPAC, 2022).

In addition to these possible modifications, the assembled device in this work can be used to manufacture and test materials. Hence, it would be possible to verify which materials are suitable to manufacturing different products, as bone screws - presented in (SÖNTGEN et al., 2022) - and catheters - as seen in (BADROU et al., 2022). In this sense, due to the currently search for materials with lower density, industries are looking for equipment and materials that favours energy efficiency and less waste emissions, as shown in (CRUZ et al., 2021). Thus, this project could be presented to test new materials.

References

ABAQUS. **Abaqus/CAE User's Manual**. Dassault Systèmes Simulia Corp, 2011. Cit. on pp. 17, 24.

ARAROMI, O.; GRAULE, M. A.; DORSEY, K.; CASTELLANOS, S.; FOSTER, J.; HSU, W.; PASSY, A.; VLASSAK, J.; WEAVER, J.; WALSH, C.; WOOD, R. Ultra-sensitive and resilient compliant strain gauges for soft machines. **Nature**, v. 587, n. 587, p. 219–224, 2020. Cit. on p. 48.

ARDUINO. **Arduino UNO R3 - Product Reference Manual**. 2022. Arduino UNO R3 - Product Reference Manual. Available from: <https://docs.arduino.cc/hardware/uno-rev3>. Visited on: 7 Sept. 2022. Cit. on p. 73.

AVIA. **HX711 24-Bit Analog-to-Digital Converter (ADC) for Weigh Scales**. 2022. HX711 Datasheet (PDF) - Avia Semiconductor Co., Ltd. Available from: <https://pdf1.alldatasheet.com/datasheet-pdf/view/1132222/AVIA/HX711.html>. Visited on: 7 Sept. 2022. Cit. on pp. 47, 48.

ÁVILA, C. T. A. **Estudo da Usinagem de Peças Impressas por Manufatura Aditiva a Arco, com Foco no Acabamento**. Sept. 2022. MA thesis – University of Brasília, Brasília. Cit. on pp. 18, 39, 42, 73.

BADROU, A.; TARDIF, N.; EVEN, A.; CHAUDET, P.; LESCANNE, N.; SZEWCZYK, J.; GRAVOUIL, A.; HAMILA, N.; BEL-BRUNON, A. Characterization of Surgical Tools for Specific Endovascular Navigation. **Cardiovascular Engineering and Technology**, v. 13, n. 5, p. 751–763, 2022. Cit. on pp. 13, 53.

BANKO, K. H. **Transfer Function Analysis of Strain Gauges**. June 2012. MA thesis – Oregon State University, Corvallis. Cit. on p. 50.

BARRANS, S. M.; MULLER, M. Finite element prediction of the ultimate axial load capacity of V-section band clamps. **Journal of Physics: Conference Series**, v. 7, n. 181, p. 1–8, 2009. Cit. on p. 13.

BARRETO, T. S. M. **Estudo das Características de Usinagem de Peças Metálicas Obtidas por Manufatura Aditiva a Arco**. May 2022. MA thesis – University of Brasília, Brasília. Cit. on pp. 18, 39, 42, 73.

BENTLEY, J. P. **Principles of Measurement Systems**. Pearson Education - London, 2005. Cit. on pp. 19, 47.

BISAGNI, C.; RAIMONDO, A.; ATANASOVSKA, I.; MILIC, M.; TROIAN, R.; FRULLA, G.; POLLA, A.; CORA, Ö.; BEKCI, M.; HENRIQUES, B.; MOURA, M. de; ALMUDAIHESH, F.; GRIGG, S. Comparison of numerical analyses of a composite wing component subjected to 4-point bending. **Composites Part C: Open Access**, v. 8, n. 100264, p. 1–8, 2022. Cit. on p. 13.

BLOMFORS, M.; LUNDGREN, K.; ZANDI, K. Incorporation of pre-existing longitudinal cracks in finite element analyses of corroded reinforced concrete beams failing in anchorage. **Structure and Infrastructure Engineering**, v. 17, n. 7, p. 960–976, 2020. Cit. on pp. 13, 17, 33.

BOUKAR, A.; CORN, S.; SLANGEN, P.; IENNY, P. Finite element modelling of low velocity impact test applied to biaxial glass fiber reinforced laminate composites. **International Journal of Impact Engineering**, v. 165, n. 104218, p. 1–8, 2022. Cit. on p. 13.

BOUVET, C.; VIEILLE, B.; PUJOLS-GONZALEZ, J. Experimental characterization and numerical modelling of the translaminar fracture of woven-ply hybrid fibers reinforced thermoplastic laminates. **Engineering Fracture Mechanics**, v. 276, n. 108867, p. 1–19, 2022. Cit. on p. 13.

CRUZ, D.; BARBOSA, M.; SANTOS, A.; MIRANDA, S.; AMARAL, R. Application of Machine Learning to Bending Processes and Material Identification. **Metals**, v. 11, n. 1418, p. 1–24, 2021. Cit. on p. 53.

EDER, M.; CHEN, X. FASTIGUE: A computationally efficient approach for simulating discrete fatigue crack growth in large-scale structures. **Engineering Fracture Mechanics**, v. 233, n. 107075, p. 1–17, 2020. Cit. on pp. 13, 15, 33.

ENERPAC. **O Cilindro Padrão de Uso Geral para a Indústria**. 2022. Cilindros Série RC-TRIO, Simples Ação. Available from: <https://www.enerpac.com/en-us/rc-series-cylinders/general-purpose-cylinder/RC51>. Visited on: 7 Sept. 2022. Cit. on pp. 21, 40, 52.

HINCHY, E.; CARCAGNO, C.; O'DOWD, N.; C.T.MCCARTHY. Using finite element analysis to develop a digital twin of a manufacturing bending operation. **Procedia CIRP Conference of Manufacturing Systems**, v. 93, n. 93, p. 568–574, 2020. Cit. on pp. 13, 15, 17, 33.

HOSFORD, W. F. **Mechanical Behavior of Materials**. Cambridge University Press - New York, 2005. Cit. on pp. 16, 17, 72.

INSTRUMENTS, N. **Measuring Strain with Strain Gages**. 2022. Strain Gauge Measurement – A Tutorial. Available from: <https://www.ni.com/pt-br/innovations/white-papers/07/measuring-strain-with-strain-gages.html>. Visited on: 7 Sept. 2022. Cit. on p. 49.

KALPAKJIAN, S.; SCHMID, S. R. **Manufacturing Processes**. Pearson, 2006. Cit. on pp. 16, 18, 25, 52.

MADSEN, N.; HAUSLADEN, M.; CHIRIAEV, S.; JOHANNESEN, P.; FABRIM, Z.; FICHTNER, P.; KJELSTRUP-HANSEN, J. Titanium Nitride as a Strain Gauge Material. **Journal of Microelectromechanical Systems**, v. 25, n. 4, p. 1–19, 2016. Cit. on pp. 48, 50.

MAKITA. **Serra Circular**. 2022. Serra Circular. Available from: <https://www.makita.com.br/catalogoFDetalhes.asp?codParamD=1250>. Visited on: 4 Dec. 2022. Cit. on p. 41.

MALCHER, L.; MORALES, L.; RODRIGUES, V.; SILVA, V.; ARAÚJO, L.; FERREIRA, G.; NEVES, R. Experimental program and numerical assessment for determination of stress triaxiality and J3 effects on AA6101-T4. **Theoretical and Applied Fracture Mechanics**, v. 106, n. 102476, p. 1–19, 2020. Cit. on p. 23.

MORI, K.; AKITA, K.; ABE, Y. Springback behaviour in bending of ultra-high-strength steel sheets using CNC servo press. **International Journal of Machine Tools & Manufacture**, v. 47, n. 47, p. 321–325, 2007. Cit. on pp. 15, 16.

OGATA, K. **Engenharia de Controle Moderno**. Pearson Education Brasil - São Paulo, 2011. Cit. on p. 18.

OMEGA. **OMEGA® STRAIN GAGES SPECIFICATIONS CHART**. 2023. OMEGA® STRAIN GAGES GENERAL PURPOSE STRAIN GAGES FOR STATIC AND DYNAMIC APPLICATIONS. Available from: <http://www.electro.fisica.unlp.edu.ar/temas/pnolo/STRAIN_GAUGES.pdf>. Visited on: 4 Feb. 2023. Cit. on p. 49.

ÖZEN, A.; ABALI, B.; VÖLLMECKE, C.; GERSTEL, J.; AUHL, D. Exploring the Role of Manufacturing Parameters on Microstructure and Mechanical Properties in Fused Deposition Modeling (FDM) Using PETG. **Applied Composite Materials**, v. 28, n. 28, p. 1799–1828, 2021. Cit. on pp. 13, 33.

RIDHA, H.; THURNER, P. Finite element prediction with experimental validation of damage distribution in single trabeculae during three-point bending tests. **Journal of the Mechanical Behavior in Biomedical Materials**, v. 27, n. 27, p. 94–106, 2013. Cit. on p. 13.

SÖNTGEN, S.; KEILIG, L.; KABIR, K.; WEBER, A.; REIMANN, S.; WELLE, K.; BOURAUEL, C. Mechanical and numerical investigations of biodegradable magnesium alloy screws for fracture treatment. **Journal of Biomedical Materials Research Part B: Applied Biomaterials**, v. 101, n. 1, p. 7–15, 2022. Cit. on pp. 13, 53.

TRZEPIECINSK, T.; LEMU, H. Effect of Computational Parameters on Springback Prediction by Numerical Simulation. **Metallurgical and Materials Transactions A**, v. 7, n. 9, p. 1–14, 2017. Cit. on pp. 24, 52.

USAINFO. **BALANÇA ARDUINO COM CÉLULA DE CARGA E HX711 – TUTORIAL CALIBRANDO E VERIFICANDO PESO**. 2023. BALANÇA ARDUINO COM ÉLULA DE CARGA E HX711 – TUTORIAL CALIBRANDO E VERIFICANDO PESO. Available from: <https://www.usinainfo.com.br/blog/balanca-arduino-com-celula-de-peso-e-hx711-tutorial-calibrando-e-verificando-peso/>. Visited on: 4 Feb. 2023. Cit. on p. 51.

VORKOV, V.; AERENS, R.; VANDEPITTE, D.; DUFLOU, J. Springback Prediction of High-strength Steels in Large Radius Air Bending Using Finite Element Modeling Approach. **Procedia Engineering**, v. 81, n. 81, p. 1005–1010, 2014. Cit. on p. 17.

Appendix

APPENDIX A – Technical Drawings used in the Metal Sheet Bending Device Project

This Appendix will show all the technical drawings developed for the metal sheet bending device project. The technical drawings have their captions in Portuguese, since they were used to present to the technicians in the SG-9 Laboratory at the University of Brasilia.

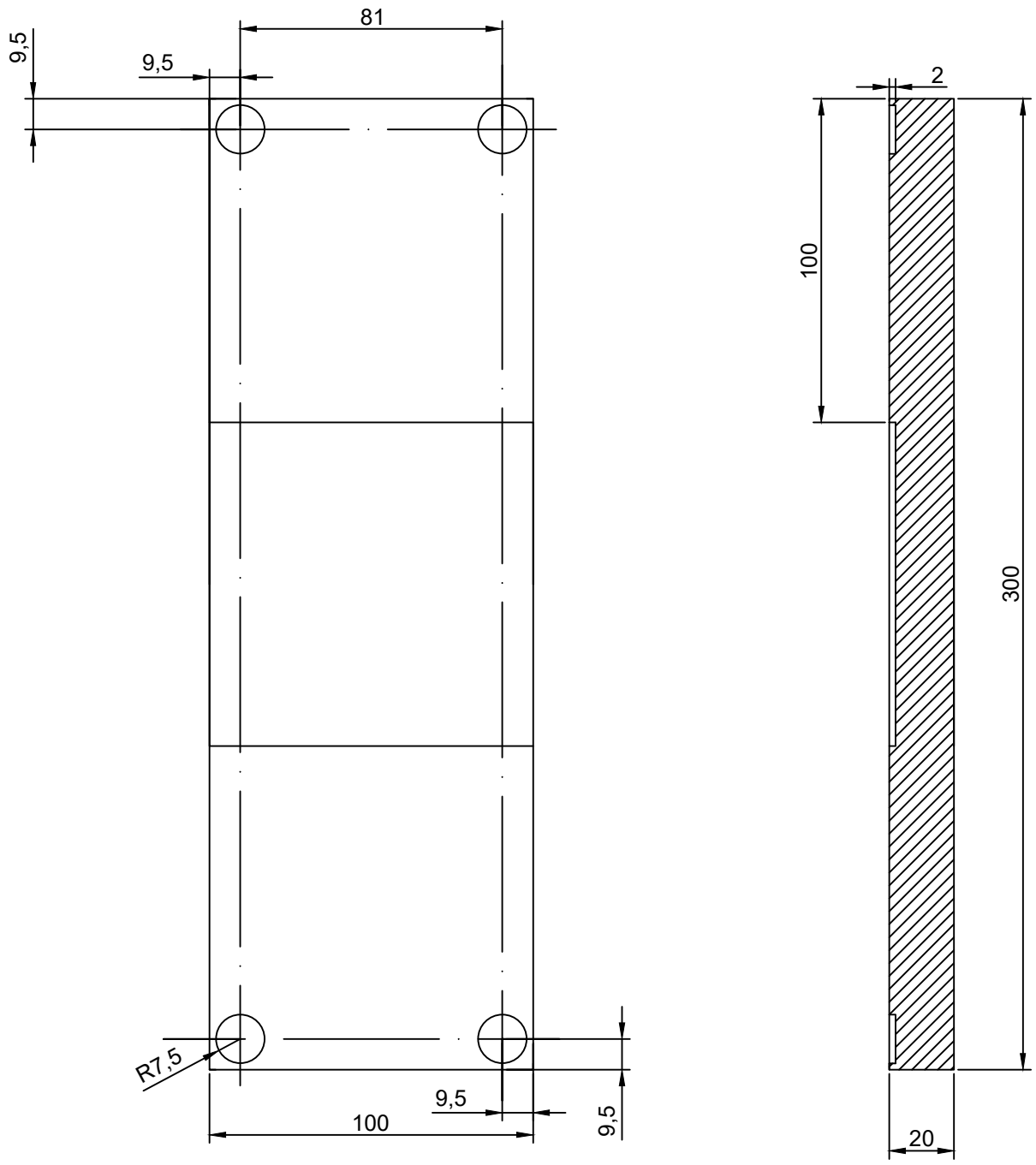

Nome da instituição: Universidade de Brasília	Data: 28/08/22	
Nome do Desenhista: Eduardo Perez Liberato	Escala: 1:2	Unidade: mm
Nome do desenho: Placa Inferior	Tamanho da folha: A4	Nº do desenho: 1

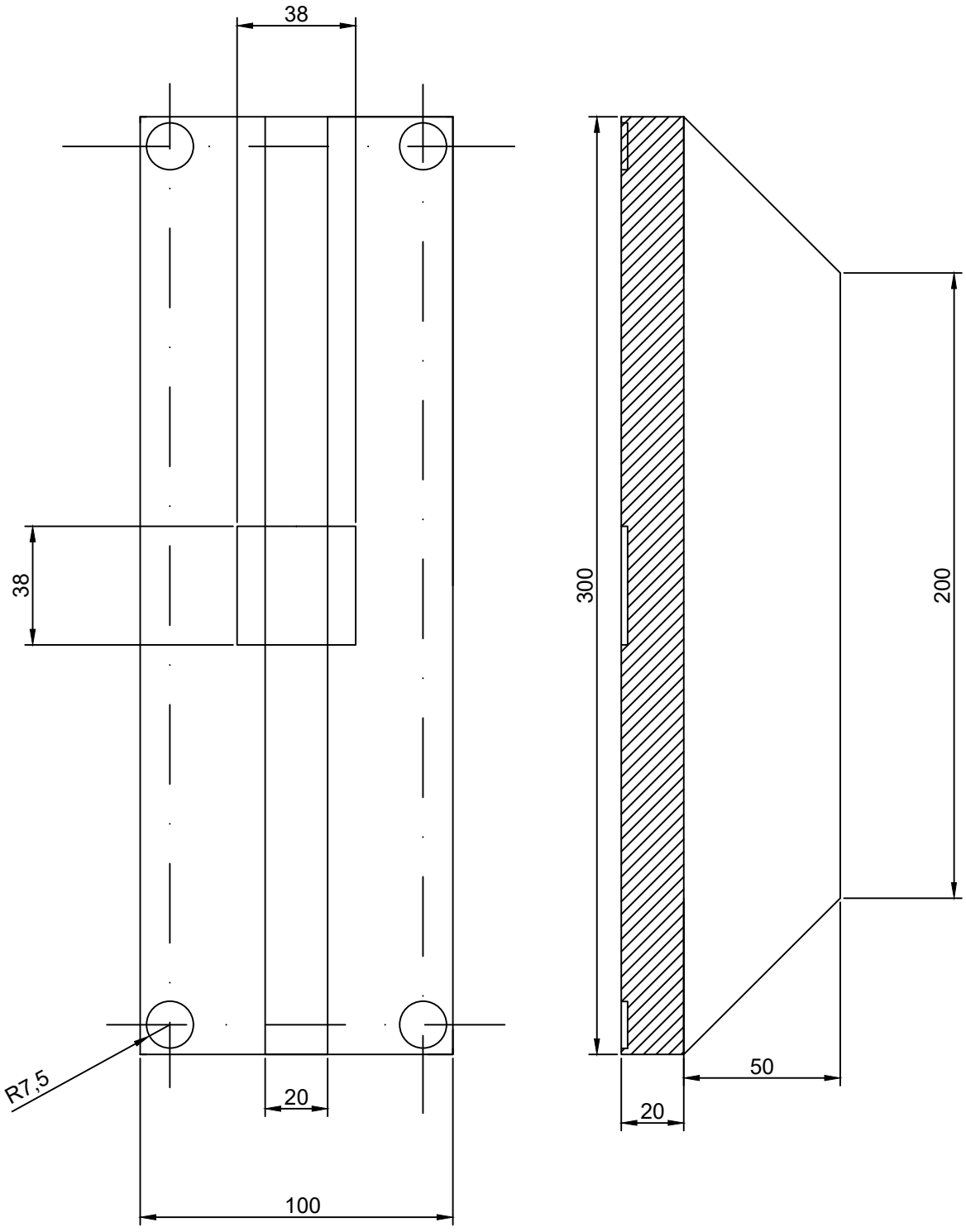

Nome da instituição: Universidade de Brasília	Data: 08/09/2022	
Nome do Desenhista: Eduardo Perez Liberato	Escala: 1:2	Unidade: mm
Nome do desenho: Placa Superior com suporte	Tamanho da folha: A4	Nº do desenho: 2

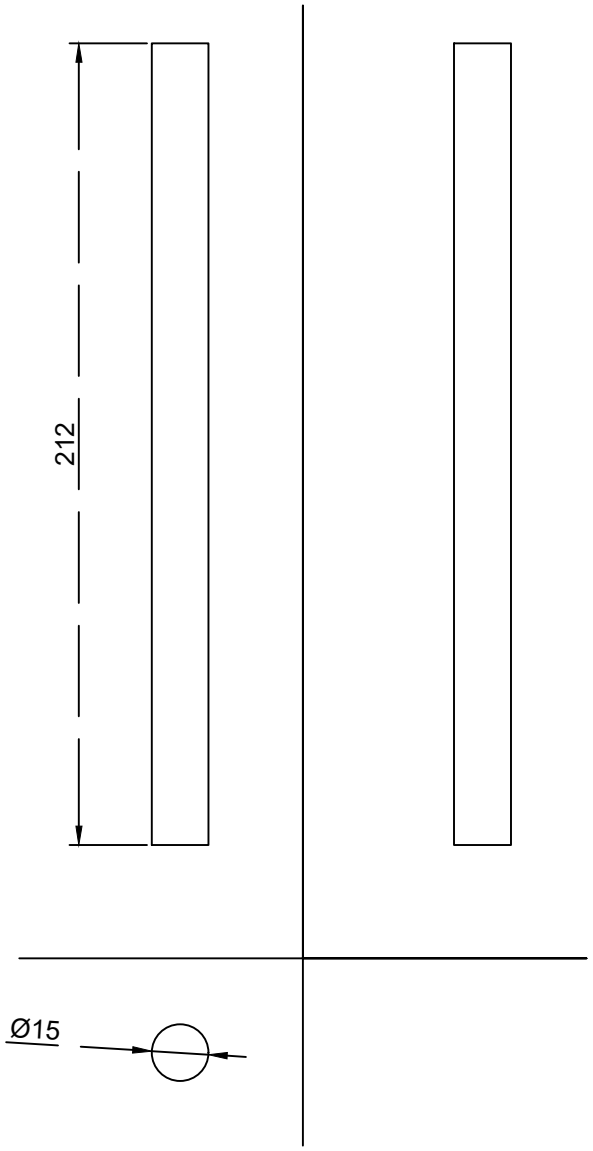

Nome da instituição: Universidade de Brasília	Data: 08/09/2022	
Nome do Desenhista: Eduardo Perez Liberato	Escala: 1:2	Unidade: mm
Nome do desenho: Barra Cilíndrica	Tamanho da folha: A4	Nº do desenho: 3

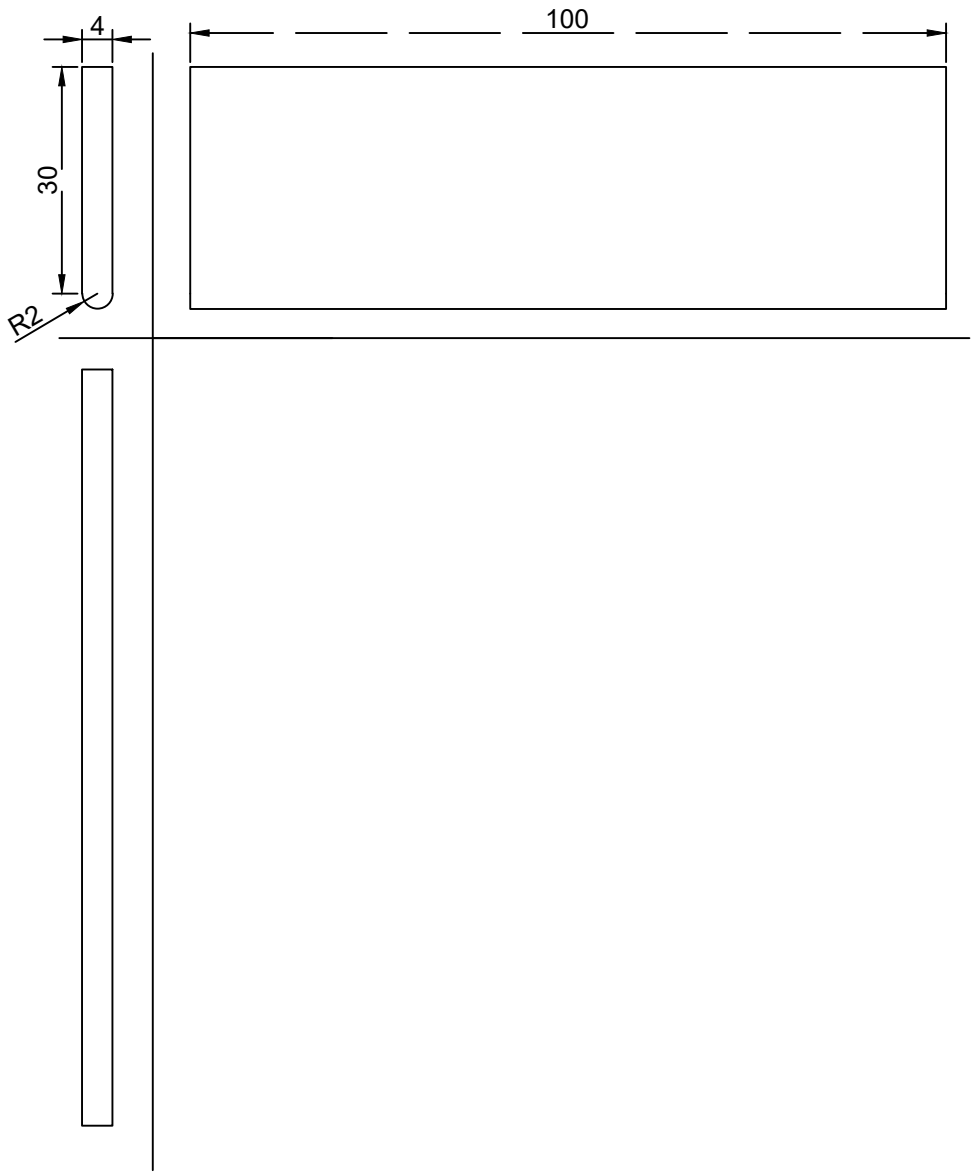

Nome da instituição: Universidade de Brasília	Data: 09/09/2022	
Nome do Desenhista: Eduardo Perez Liberato	Escala: 1:1	Unidade: mm
Nome do desenho: Punção	Tamanho da folha: A4	Nº do desenho: 4

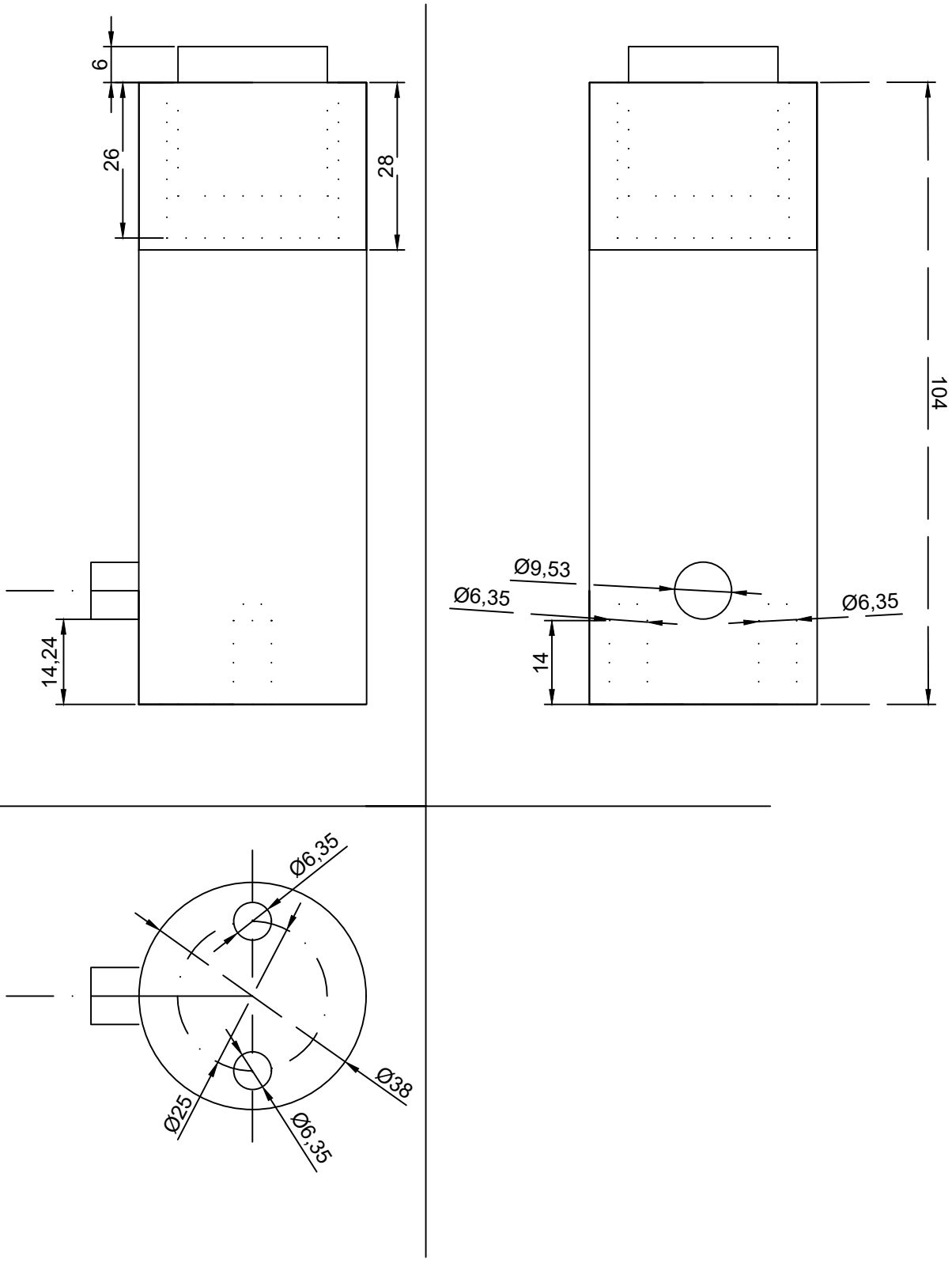

Nome da instituição: Universidade de Brasília	Data: 10/09/2022	
Nome do Desenhista: Eduardo Perez Liberato	Escala: 1:1	Unidade: mm
Nome do desenho: Atuador Enerpac RC-51	Tamanho da folha: A4	Nº do desenho: 5

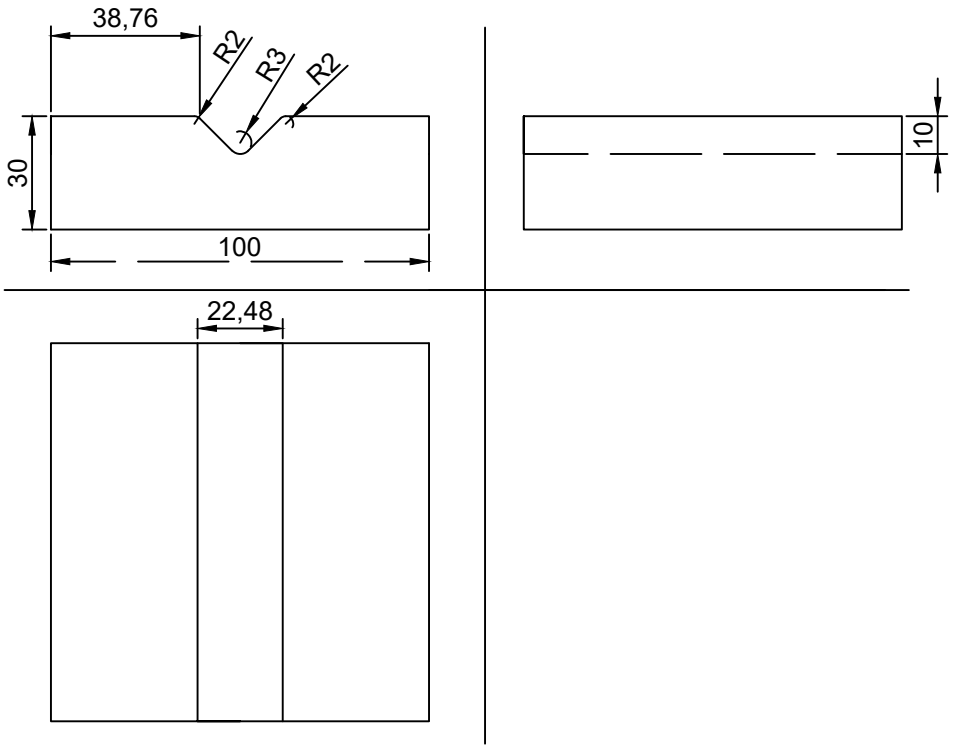

Nome da instituição: Universidade de Brasília	Data: 10/09/2022	
Nome do Desenhista: Eduardo Perez Liberato	Escala: 1:2	Unidade: mm
Nome do desenho: Molde 1 mm	Tamanho da folha: A4	Nº do desenho: 6

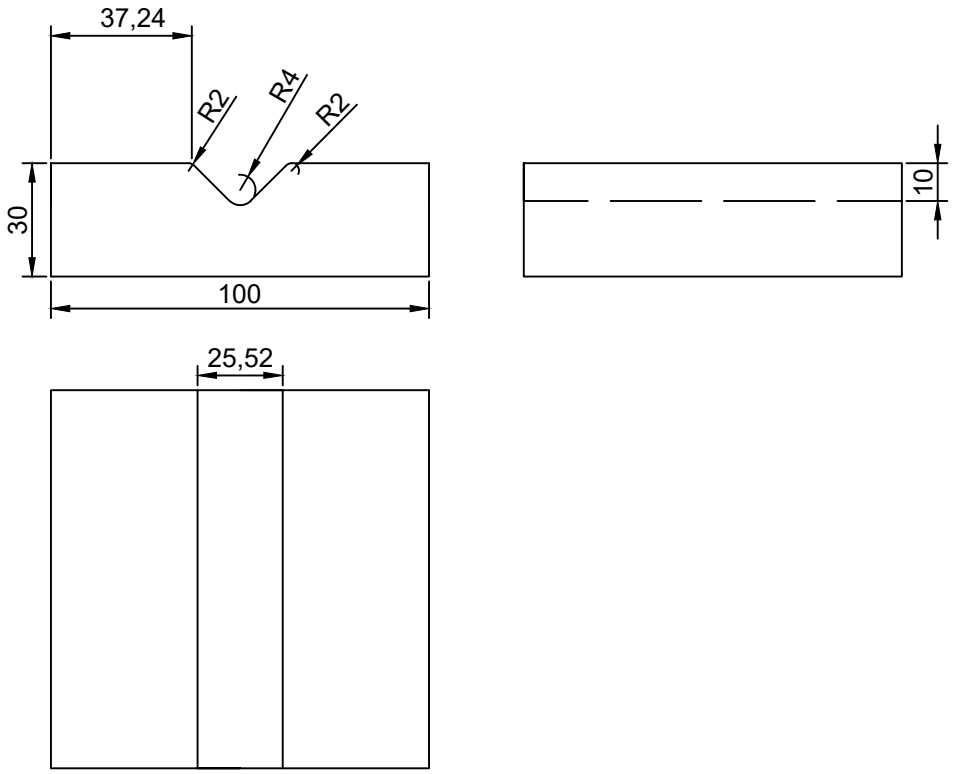

Nome da instituição: Universidade de Brasília	Data: 10/09/2022	
Nome do Desenhista: Eduardo Perez Liberato	Escala: 1:2	Unidade: mm
Nome do desenho: Molde 2 mm	Tamanho da folha: A4	Nº do desenho: 7

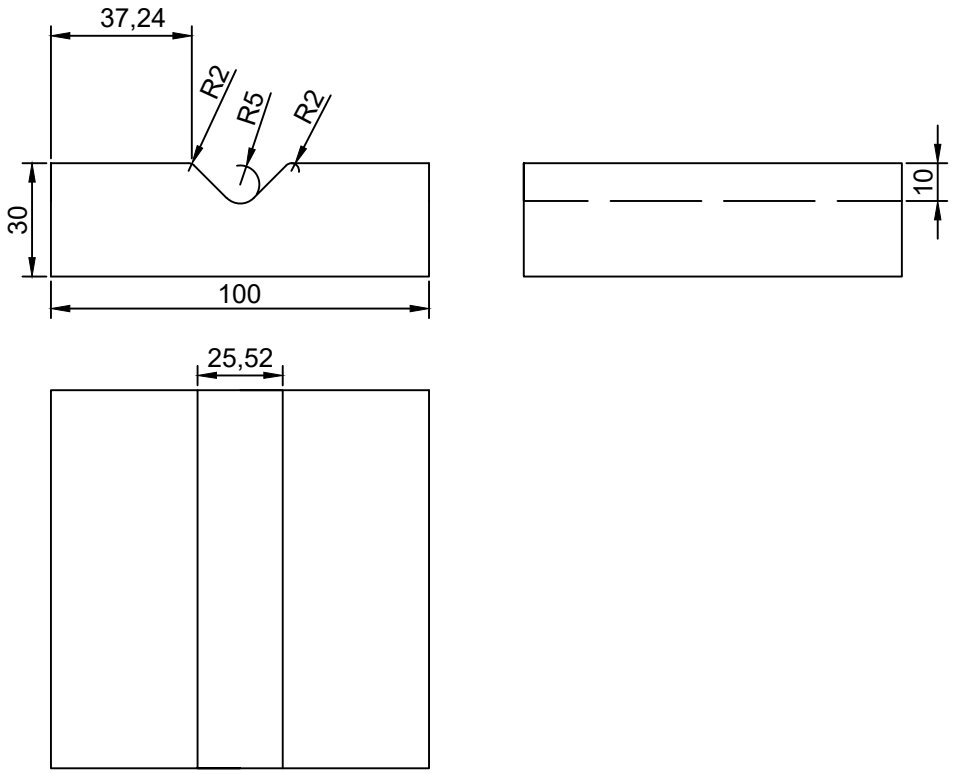

Nome da instituição: Universidade de Brasília	Data: 10/09/2022	
Nome do Desenhista: Eduardo Perez Liberato	Escala: 1:2	Unidade: mm
Nome do desenho: Molde 3 mm	Tamanho da folha: A4	Nº do desenho: 8

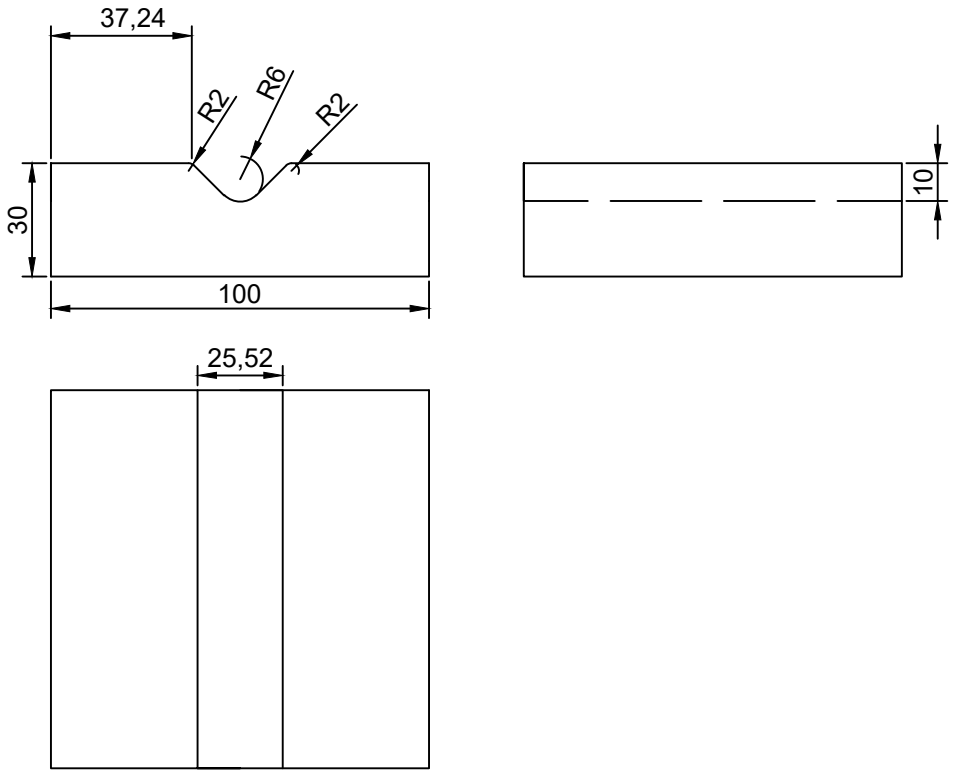

Nome da instituição: Universidade de Brasília	Data: 10/09/2022	
Nome do Desenhista: Eduardo Perez Liberato	Escala: 1:2	Unidade: mm
Nome do desenho: Molde 4 mm	Tamanho da folha: A4	Nº do desenho: 9

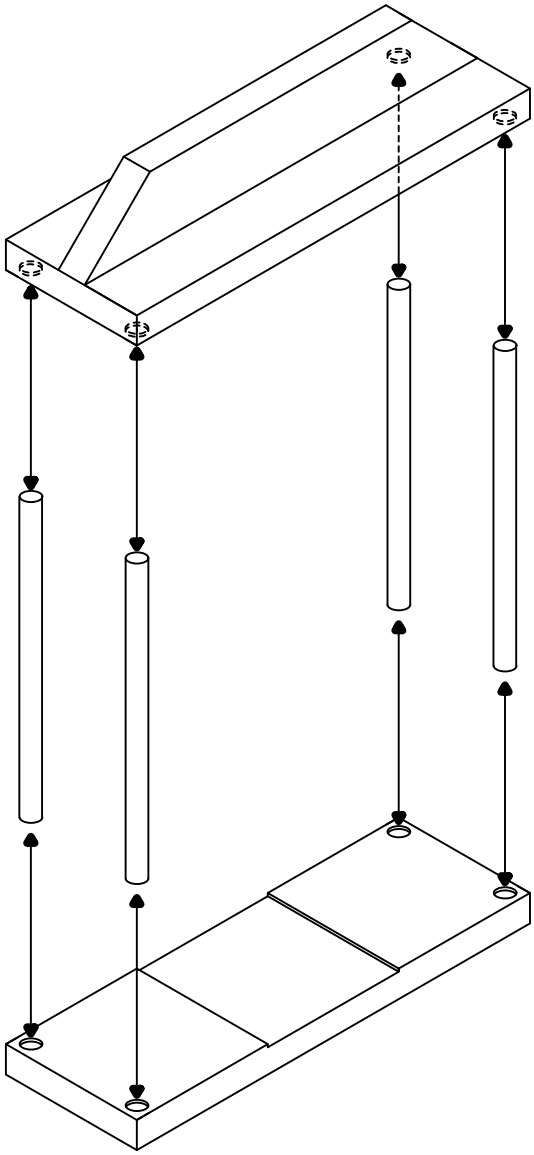

Nome da instituição:	Data:	
Universidade de Brasília	28/11/22	
Nome do Desenhista:	Escala:	Unidade:
Eduardo Perez Liberato	1:5	mm
Nome do desenho:	Tamanho da folha:	Nº do desenho:
Desenho de montagem do Chassi	A4	10

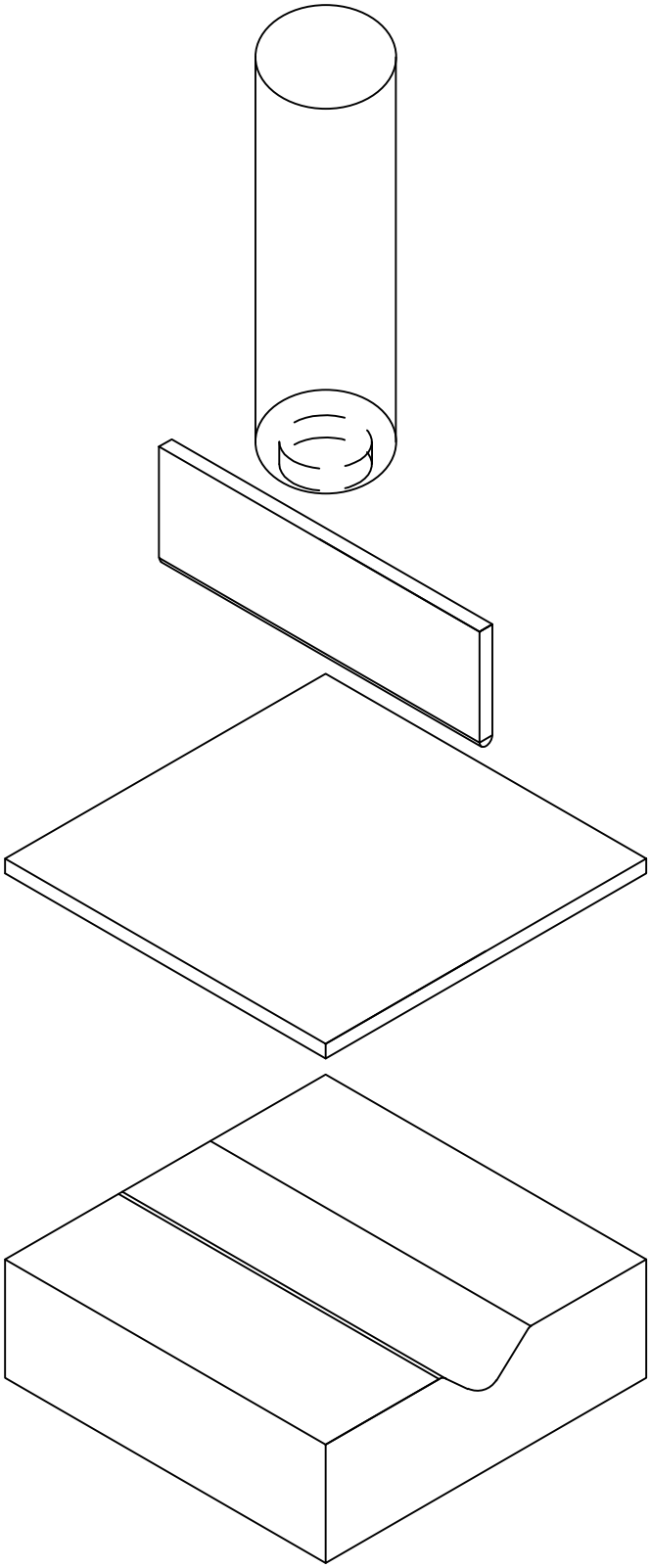

Nome da instituição:	Data:	
Universidade de Brasília	30/11/2022	
Nome do Desenhista:	Escala:	Unidade:
Eduardo Perez Liberato	1:2	mm
Nome do desenho:	Tamanho da folha:	Nº do desenho:
Desenho de montagem do sistema de dobra	A4	11

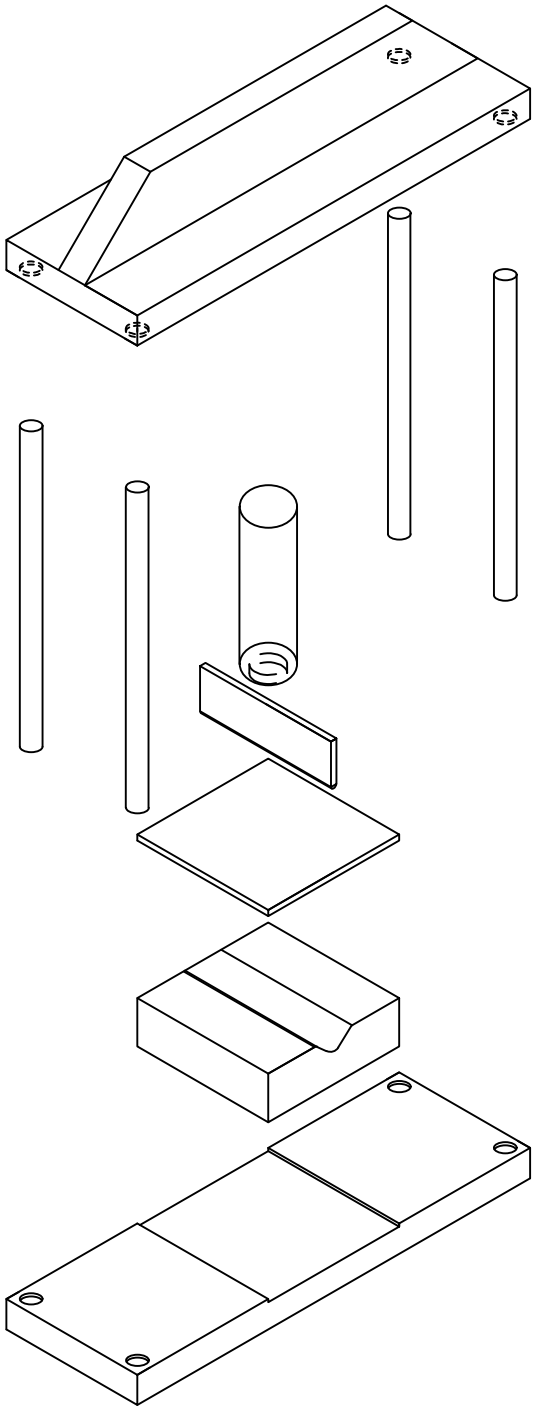

Nome da instituição: Universidade de Brasília	Data: 30/11/2022	
Nome do Desenhista: Eduardo Perez Liberato	Escala: 1:5	Unidade: mm
Nome do desenho: Desenho explodido de montagem do equipamento completo	Tamanho da folha: A4	Nº do desenho: 12

APPENDIX B – Tables

Table 5 – Stress-strain curve for the aluminium A6101-T4 used as the metal sheet's base material.

Yield Stress [Pa]	Plastic Strain (E [mm])
96	0
110,8629395	0,01
124,1040351	0,02
135,908122	0,03
146,4389705	0,04
155,8416863	0,05
164,2448385	0,06
171,7623431	0,07
178,4951341	0,08
184,5326421	0,09
189,9541057	0,1
210,0164304	0,15
222,4063576	0,2
230,6065849	0,25
236,5189241	0,3
245,1626462	0,4
252,1755738	0,5
258,7022029	0,6
265,0838191	0,7
271,4221929	0,8
277,747672	0,9
284,0693058	1
290,389793	1,1
296,7099383	1,2
303,0299816	1,3
309,3499945	1,4
315,6699984	1,5

Source: (HOSFORD, 2005)

Table 6 – Cutting Fluid BIO100E (1:9) Information used in the milling process

Parameter	Specification
Rotations per minute (RPM)	1740 rpm
Minimum Forward Speed (V_{fmax})	56 mm/min
Maximum Forward Speed (V_{fmin})	28 mm/min
Minimum Cutting Speed (V_{Cmax})	56 mm/min
Maximum Cutting Speed (V_{Cmin})	28 mm/min
Minimum Cut Depth (a_{pmin})	0,5 mm
Maximum Cut Depth (a_{pmax})	2 mm
Visual Aspect	Greenish Yellow
Density 20/4 C - NBR 7148	1,065 g/cm^3
Refractive index - MT 29	3,33
pH (3% in the water) - MT 6	9,5
Corrosion in Cast Iron GG 25 sol.3% _ DIN 51.3560/2	No corrosion detected

Source: (ÁVILA, 2022) and (BARRETO, 2022)

Table 7 – Arduino UNO's Information

Abreviation	Description	Minimum	Maximum	Unity
	Board's Thermal Limit	-45	85	°C
VINMax	Maximum Input Computer's Voltage	6	20	V
VUSBMax	Maximum Input Arduino's Voltage by USB port		5.5	V

Source: (ARDUINO, 2022)